

AFFDL-TR-75-123
ADA 025 266

ANALOG COMPUTATION ASSESSMENT OF THE RISK OF STRUCTURAL FAILURE DUE TO CRACK GROWTH UNDER RANDOM LOADING

*AEROELASTIC AND STRUCTURES RESEARCH LABORATORY
DEPARTMENT OF AERONAUTICS AND ASTRONAUTICS
MASSACHUSETTS INSTITUTE OF TECHNOLOGY
CAMBRIDGE, MASSACHUSETTS 02139*

OCTOBER 1975

TECHNICAL REPORT AFFDL-TR-75-123
FINAL REPORT FOR PERIOD FEBRUARY 1974 — MAY 1975

Approved for public release; distribution unlimited

AIR FORCE FLIGHT DYNAMICS LABORATORY
AIR FORCE WRIGHT AERONAUTICAL LABORATORIES
Air Force Systems Command
Wright-Patterson Air Force Base, Ohio 45433

Best Available Copy

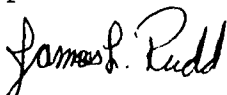
20060921136

NOTICE

When Government drawings, specifications, or other data are used for any purpose other than in connection with a definitely related Government procurement operation, the United States Government thereby incurs no responsibility nor any obligation whatsoever; and the fact that the Government may have formulated, furnished, or in any way supplied the said drawings, specifications, or other data, is not to be regarded by implication or otherwise as in any manner licensing the holder or any other person or corporation, or conveying any rights or permission to manufacture, use, or sell any patented invention that may in any way be related thereto.

This report has been reviewed by the Information Office (OI) and is releasable to the National Technical Information Service (NTIS). At NTIS, it will be available to the general public, including foreign nations.

This technical report has been reviewed and is approved for publication.



JAMES L. RUDD
Project Engineer
Fatigue, Fracture & Reliability Gp




HOWARD A. WOOD, Principal Scientist
Structural Integrity Branch
Structures Division



ROBERT M. BADER, Chief
Structural Integrity Branch
Structures Division

FOR THE COMMANDER



GERALD G. LEIGH, Lt Col, USAF
Chief, Structures Division

Copies of this report should not be returned unless return is required by security considerations, contractual obligations, or notice on a specific document.

UNCLASSIFIED

SECURITY CLASSIFICATION OF THIS PAGE (When Data Entered)

REPORT DOCUMENTATION PAGE		READ INSTRUCTIONS BEFORE COMPLETING FORM
1. REPORT NUMBER AFFDL-TR-75-123	2. GOVT ACCESSION NO. N/A	3. RECIPIENT'S CATALOG NUMBER N/A
4. TITLE (and Subtitle) ANALOG COMPUTATION ASSESSMENT OF THE RISK OF STRUCTURAL FAILURE DUE TO CRACK GROWTH UNDER RANDOM LOADING		5. TYPE OF REPORT & PERIOD COVERED FINAL Feb. 1974 - May 1975
7. AUTHOR(s) Oscar Orringer Richard F. Harris John F. McCarthy, Jr.		6. PERFORMING ORG. REPORT NUMBER ASRL TR 179-1
9. PERFORMING ORGANIZATION NAME AND ADDRESS Aeroelastic and Structures Research Lab. Massachusetts Institute of Technology Cambridge, Massachusetts 02139		8. CONTRACT OR GRANT NUMBER(s) F33615-74-C-3046
11. CONTROLLING OFFICE NAME AND ADDRESS Air Force Flight Dynamics Laboratory Air Force Systems Command Wright-Patterson AFB, Ohio 45433		10. PROGRAM ELEMENT, PROJECT, TASK AREA & WORK UNIT NUMBERS 19290107
14. MONITORING AGENCY NAME & ADDRESS (if different from Controlling Office) Same		12. REPORT DATE October 1975
		13. NUMBER OF PAGES 89
		15. SECURITY CLASS. (of this report) Unclassified
		15a. DECLASSIFICATION/DOWNGRADING SCHEDULE N/A
16. DISTRIBUTION STATEMENT (of this Report) Approved for public release; distribution unlimited.		
17. DISTRIBUTION STATEMENT (of the abstract entered in Block 20, if different from Report) Same		
18. SUPPLEMENTARY NOTES None		
19. KEY WORDS (Continue on reverse side if necessary and identify by block number) Risk Analysis Random Load Fatigue Crack Growth Safety		
20. ABSTRACT (Continue on reverse side if necessary and identify by block number) Risks of fracture were computed from a Monte Carlo simulation of the Paris equation for crack growth rate. The simulation covered a total number of load events approximately equivalent to the estimated useful service life for a typical fighter airplane. The simulation was implemented by development of a computation technique based on the analog computer. Approximately 200 simulations were run for each of 11 assumed initial crack sizes, with the loading represented by a random noise signal filtered through a track-hold circuit to match a		

DD FORM 1473

1 JAN 73

EDITION OF 1 NOV 65 IS OBSOLETE

UNCLASSIFIED

SECURITY CLASSIFICATION OF THIS PAGE (When Data Entered)

UNCLASSIFIED

SECURITY CLASSIFICATION OF THIS PAGE(When Data Entered)

stress range exceedance distribution derived from an acceleration peak exceedance curve for the typical aircraft fleet. The resulting data were sampled at four fractions of simulated service life and then reduced to four final crack size histograms for each initial crack size. The raw data histograms were used to estimate parameter values for three-parameter Weibull distributions for final crack size in each case, and a regression analysis was performed to correlate the distributions for risk analysis. Mathematical risks of structural failure were computed and compared for several combinations of assumptions about the loading and the initial crack size distributions.

UNCLASSIFIED

SECURITY CLASSIFICATION OF THIS PAGE(When Data Entered)

FOREWORD

The developments documented in this report were carried out at the Aeroelastic and Structures Research Laboratory, Massachusetts Institute of Technology, Cambridge, Massachusetts 02139, under Contract No. F33615-74-C-3046 (Project/Task 1929/01) from the U.S. Air Force Flight Dynamics Laboratory. Mr. Howard A. Wood (AFFDL/FBE) served as technical monitor. Many valuable suggestions were also contributed by Mr. Charles F. Tiffany (ASD/EN) and Captain Daniel Hayes (AFFDL/FBE). The research was carried out from February 1974 through May 1975 and was originally submitted by the author in June 1975.

TABLE OF CONTENTS

	<u>Page</u>
1 INTRODUCTION	1
1.1 Monte Carlo Method	1
1.2 Constant Sinusoidal Amplitude Problem	3
2 ANALOG COMPUTER PROGRAMMING OF THE PARIS GROWTH EQUATION	6
2.1 The Analog Computer	6
2.2 Paris Equation for Constant Load	8
2.3 Random Load Simulation	10
2.4 Track-Hold Noise	10
2.5 Paris Solution for Random Loading	12
2.6 Repetitive Operation (REPOP)	13
2.7 Errors and Special Circuitry	14
2.8 Sample Monte Carlo Run	17
3 EXTENDED MONTE CARLO SIMULATION	18
3.1 The Computation Problem and Its Solution	18
3.2 Description of the Monte Carlo Simulation	22
3.3 Risk Sensitivity Assessment	27
4 DISCUSSION AND CONCLUSIONS	33
REFERENCES	37
TABLES	38
FIGURES	54

LIST OF TABLES

<u>Table</u>		<u>Page</u>
1	Common Linear Analog Components	38
2	Common Nonlinear Analog Components	40
3	Weibull Shape Parameter $\hat{\alpha}$ for Final Crack Size Distribution	44
4	Weibull Scale Parameter $\hat{\beta}$ (Mils) for Final Crack Size Distribution	45
5	Risk $R_f(a_{cr} a_i, v)$ for $a_{cr} = 122$ Mils	46
6	Combined Risk for a_i to $a_{cr} = 122$ Mils	47
7	Crack Growth Behavior under Central Loading	48
8	Hypothetical Distributions for Initial Flaws	49
9	Combined Risk for a_i to a_{cr} (CV = 0.2)	50
10	Combined Risk for a_i to a_{cr} (CV = 0.3)	51
11	Combined Risk for a_i to a_{cr} (CV = 0.4)	52
12	Comparison of Risks to 122 Mils	53

LIST OF ILLUSTRATIONS

<u>Figure</u>		<u>Page</u>
1	Weibull Distribution for Crack Size as a Function of Constant-Amplitude Fatigue	54
2	Paris Equation Analog Program Diagram	55
3	Typical Analog Crack Growth Solution for Constant-Amplitude Fatigue	56
4	Gaussian Noise Generator Circuit	57
5	Samples of Track-Hold Noise	58
6	Analog Program Diagram for Mean and Standard Deviation	59
7	Analog Program Diagram for Paris Equation with Random Loading	60
8	Typical Analog Crack Growth Solution for Random-Load Fatigue	61
9	Typical Analog Random-Load Solution Using REPOP	62
10	REPOP Switch Error	63
11	Analog Program Diagram for Paris Equation with Random Loading and Rescaling . .	64
12	Histogram of Crack Size after 10,000 Fatigue Cycles	65
13	Histogram of Crack Size after 15,000 Fatigue Cycles	66
14	Histogram of Crack Size after 20,000 Fatigue Cycles	67
15	Crack Size Histogram ($a_i=.03$, $N=8,000$)	68
16	Crack Size Histogram ($a_i=.03$, $N=10,000$)	69
17	Crack Size Histogram ($a_i=.03$, $N=13,300$)	70

LIST OF ILLUSTRATIONS
(continued)

<u>Figure</u>	<u>Page</u>
18 Crack Size Histogram ($a_i=.03$, $N=20,000$)	71
19 Crack Size Histogram ($a_i=.04$, $N=8,000$)	72
20 Crack Size Histogram ($a_i=.04$, $N=10,000$)	73
21 Crack Size Histogram ($a_i=.04$, $N=13,300$)	74
22 Crack Size Histogram ($a_i=.04$, $N=20,000$)	75
23 Crack Size Histogram ($a_i=.05$, $N=8,000$)	76
24 Crack Size Histogram ($a_i=.05$, $N=10,000$)	77
25 Crack Size Histogram ($a_i=.05$, $N=13,300$)	78
26 Crack Size Histogram ($a_i=.05$, $N=20,000$)	79
27 Crack Size Histogram ($a_i=.06$, $N=8,000$)	80
28 Crack Size Histogram ($a_i=.06$, $N=10,000$)	81
29 Crack Size Histogram ($a_i=.06$, $N=13,300$)	82
30 Crack Size Histogram ($a_i=.07$, $N=8,000$)	83
31 Crack Size Histogram ($a_i=.07$, $N=10,000$)	84
32 Crack Size Histogram ($a_i=.07$, $N=13,300$)	85
33 Crack Size Histogram ($a_i=.07$, $N=20,000$)	86
34 Correlation of Final Crack Size Distribution Scale Parameters	87
35 Typical Detection Probability Curves	88
36 Reshaping of Flaw Creation Probability by Inspection Reliability	89
37 Schematic for Computation of Combined Failure Risk	89

Section 1

INTRODUCTION

1.1 Monte Carlo Method

With longevity or durability requirements being incorporated in the structural design of aircraft, analysis of structural failure due to fatigue has become an important design criterion. One aspect of structural life analysis is the growth of minute material flaws in the stressed material which after some time grow to a critical size due to load cycling under normal flight conditions. This fatigue load history for an aircraft is the sum of several load sources. Ground-air-ground cycles, wind gusts, maneuver loads and engine noise all contribute to the fatigue loading and may cause material flaws to grow to a dangerously critical size.

Current methods of predicting when the cracks will grow critical, or what size they will reach after a given number of flight hours, leave much to be desired since even the model of crack growth due to simple constant sinusoidal amplitude fatigue is a controversial subject. The present scheme of crack growth prediction due to expected flight loadings is to choose a crack growth model and a "representative" load spectrum for one or more flights. Crack growth due to the pseudorandom history is then computed over several flights. An example of such a digital computer program is the Air Force CRACKS II program [1]. Results from such a scheme can give accurate solutions for many deterministic cases, but a more precise and truly random load history is required to properly

predict crack growth dispersion. Such a program would require the random generation of the load spectrum expected in real flight conditions containing ground-air-ground (GAG) cycles, random or deterministic maneuver loads, random gust loads, etc. This would involve knowledge of, for example, the expected number or spectrum of maneuver loads as well as a spectrum model for the turbulent gust loads. Combined spectra which include all of these sources may be deduced from experimental data sampled from aircraft flight histories.

Since each crack growth solution over a finite load history would be unique, many crack growths would have to be computed to obtain a distribution of crack size solutions which could be used in risk assessment evaluation of the structure. In addition to the loads being random, the sizes of the initial flaws or crack sizes in the material are also random in nature. Introduction of the initial crack size as an additional random variable can also be required for more realistic growth calculations. Other random structural properties may also be introduced into the problem, such as construction and inspection reliability factors.

After the introduction of appropriate random variables, the computation of crack growth due to the simulated environment can be repeated a sufficient number of times to represent the life or partial life of the aircraft, thus producing a final probability distribution of crack sizes in a particular structural member from a Monte Carlo simulation. If the computation of each growth problem is cheap enough, the Monte Carlo technique can be used as a practical approach to fatigue damage estimation.

The reduced cost of the analog approach to crack growth computation is considered to be most useful for trade-off studies in which fatigue damage risks may be assessed in aircraft fleets for which usage (spectrum) variation is considered. However, the limited scope of the present study required restriction to one load spectrum, the primary objective having been to demonstrate the technical feasibility of the analog method.

1.2 Constant Sinusoidal Amplitude Problem

It is possible to obtain a closed form solution for the distribution of crack sizes in a structure after constant amplitude fatigue, given an initial crack distribution, by making use of a technique of variable transformation [2]. Computing crack growth due to the sinusoidal fatigue loading will result in a shifting and reshaping of the initial flaw distribution as a function of time. If all cracks grew at the same rate, the crack distribution would only shift on the crack size axis and keep its original shape, but in reality, larger cracks grow faster than smaller ones. Hence, a reshaping is also seen in the form of a wider dispersion at larger crack sizes. The variable transformation is accomplished in the following way. Let a_0 be a random initial crack size with probability density function $f_0(a_0)$ and $a = g(a_0)$, where $g(a_0)$ is the final size of any initial crack of size a_0 .

Then:

$$f(a) = f_0[g^{-1}(a)] \left| \frac{da_0}{da} \right| \text{ or } f(a) = f_0[g^{-1}(a)] \left| \frac{dg}{da_0} \right|^{-1} \quad (1)$$

For example, if a Weibull distribution for initial crack size and the Paris growth model [3] are assumed such that

$$f_0(a_0) = \frac{\alpha}{\beta^\alpha} a_0^{\alpha-1} e^{-(a_0/\beta)^\alpha}; \quad a_0, \alpha, \beta > 0 \quad (2)$$

where

a_0 = initial crack size at $N = 0$

α, β = given parameters for a Weibull distribution

N = number of fatigue cycles

and

$$da/dN = C_p (\Delta K)^{2r} \approx C_p \Delta \sigma^{2r} a^r = C a^r \quad (3)$$

and where C_p and r are material constants, then the Paris growth solution is given by

$$a_0 = [a^{1-r} + (r-1)CN]^{1/(1-r)} \quad (4)$$

Now substituting Eq. 2 and Eq. 4 into Eq. 1 we have

$$f(a) = \frac{\alpha}{\beta^\alpha a^r} [a^{1-r} + (r-1)CN]^{-\left(\frac{\alpha+r-1}{r-1}\right)} \exp\left\{-\frac{[a^{1-r} + (r-1)CN]^{-\left(\frac{\alpha}{r-1}\right)}}{\beta^\alpha}\right\} \quad (5)$$

When $N = 0$, $f(a)$ reduces to $f_0(a_0)$. For N very large, $f(a) \rightarrow 0$ or almost all cracks have grown to critical size. See Fig. 1 for typical solutions. When $\Delta\sigma$ is a random variable, the variable transformation becomes quite difficult to use because integration of the growth model over the random load is tedious. Thus, when considering a more realistic loading environment, the Monte Carlo method could be employed.

The analog computer is a good choice to facilitate such a scheme, provided that computation costs are reasonable. Digital computers will suffice for numerical integration of the growth model and random variable generation as well. However, digital computer costs would be quite high for a full-range parameter study of initial crack sizes, material constants and a reasonable range of load cases. Since the growth equations are primarily nonlinear first order differential equations, the high speed analog computer offers a practical solution procedure at potentially only a fraction of the digital computer costs. The random load simulation can be accomplished by introducing random noise generators with appropriate statistics for the fatigue environment. Additional generators can be employed for other nonrandom load sources. An analog computer Monte Carlo scheme has been developed to calculate the distributions of crack growth sizes due to random fatigue loads. The resulting computational costs are several orders of magnitude less than traditional digital schemes. The development of the method is the significant feature and not the validity of any particular crack growth model or any specific random load model. For illustrative purposes, the Paris crack growth equation is used throughout with Gaussian noise as the random loading $\Delta\sigma$.

Section 2

ANALOG COMPUTER PROGRAMMING OF THE PARIS GROWTH EQUATION

2.1 The Analog Computer

The development of analog computer technology can be attributed to electronics advances during World War II [4]^{*}. Because of the tremendous popularity that digital computers have acquired recently in terms of data handling capacity and computation speed, the analog has been neglected altogether in many cases as an efficient computing device. Today there exist many high speed repetitive-operation analog computers capable of solving linear and non-linear higher-order differential equations. Although digitals by nature are capable of better computing accuracy than analog computers, the analog is capable of continuous function integration and differentiation which digital computers find difficult to perform.

In terms of major computation costs, the analog computer's initial machine cost must be compared with digital computation rates and rentals. The cost of an analog computer may range from a simple twenty-dollar circuit to a several-hundred-thousand dollar facility, depending on the computer's capabilities. The analog computer used in this study is an Electronic Associates, Inc., TR-48 PACE^{**}.

^{*} Reference 4 contains an excellent analog computer method review.

^{**} This facility is of 1960 vintage and cost about \$25,000 at that time.

The fundamental feature of most analog computers is the patch board which contains an array of components which are connected by wires in a specific sequence determined by the particular computer program. The basic components consist of integrators, inverters, summers, multipliers, logic circuits, etc., which determine the overall capability of the computer. The fundamental circuit component of the analog computer is the operational amplifier (OPAMP) which is used in the summers, inverters and integrators, as well as in other devices. By connecting a feedback resistor across the OPAMP and adding an input resistor, the OPAMP becomes a summer of all inputs into the input resistor with gain determined by the ratio of the feedback resistor to the input resistor. The inverter is actually a summer with only one input since the OPAMP output is the negative of its input. Integration is accomplished by replacing the feedback resistor with a feedback capacitor. If $x(t)$ is the integrator input, the output will be $-\frac{1}{RC} \int_0^T x(t) dt + V_0$ where

V_0 = initial condition of the integrator = $x(0)$

R = input resistance

C = feedback capacitance

If RC is variable, the integration rate or time scale can be adjusted such that a problem taking several minutes to solve in real time requires only a few milliseconds with proper RC values (time scaling). Table 1 summarizes some of the most common component devices used in analog programming. Nonlinear devices such as multipliers, squares, dividers and function generators are also available in most analog component boards. The most common nonlinear circuits are listed in Table 2.

In analog programming, variable scaling is required for accurate problem solutions. The independent variables of the equations are represented on the analog computer by time. The dependent variables and their derivatives with respect to time are represented by voltages. These signal voltages must not exceed the maximum allowed machine voltage^{*}, nor should they change rapidly enough to exceed the frequency limitations of the computer or recording equipment. In addition, the voltages should not be as small as the order of circuit errors, and the problem solution time should not be so long as to waste computer efficiency. By scaling the problem properly, rapid, accurate solutions can be obtained by appropriate voltage variables and solution speeds.

2.2 Paris Equation for Constant Load

The first step in setting up the Monte Carlo method is to choose a crack growth model. The Paris equation has been chosen for the sake of simplicity. The Paris growth equation is given by:

$$da/dN = C_p (\Delta K)^{N_p} \approx C_p \Delta \sigma^{N_p} a^{N_p/2} \quad (6)$$

Typical values for N_p and C_p for aluminum are $N_p \approx 4$ and $C_p = 3.49 \times 10^{-10}$ to 3.91×10^{-9} , where a is in inches and $\Delta \sigma$ is in ksi^{**}. N_p has been chosen as a multiple of 2 so that circuit squaring devices can be conveniently used in the problem patching.

^{*}In the case of the TR-48, ±10 volts.

^{**}Parameters obtained by fitting experimental da/dN data [5].

For a constant $\Delta\sigma$, the problem is quite trivial resulting in the solution:

$$\frac{1}{a} = \frac{1}{a_0} - C_p \Delta\sigma^4 N \quad (7)$$

where a_0 is the initial crack size at $N = 0$. The nature of this family of solutions is that of an increasing exponential curve which presents three major problems on the analog computer:

1. Without careful selection of the solution time or length, several orders of magnitude of crack growth can result which would obviously exceed the maximum voltage limits.
2. Minute errors during the first portion of the solution can grow significantly by the end of the problem.
3. Since the growth rate is proportional to $\Delta\sigma^4$, very rapid crack growths may result.

With proper time and variable scaling, all of these difficulties can be overcome.

The symbolic analog programming diagram for the Paris growth equation for $N_p = 4$ is given in Fig. 2. A typical analog growth solution recorded on chart paper is given in Fig. 3. The values of $\Delta\sigma$ and a are recorded on the same two-channel recorder for comparison. A quick calculation shows the exact analytical solution for a crack to grow from 0.1 inch to 1.0 inch for $C_p = 3.488 \times 10^{-10}$, $N_p = 4$ and $\Delta\sigma = 50$ ksi is 4128 fatigue cycles. The analog solution gives 4130, verifying the accuracy of the analog program. It is quite easy to see that $\Delta\sigma$ can now be a random variable of time rather than just a constant.

2.3 Random Load Simulation

One of the advantages of using the analog rather than the digital computer for growth calculations is the ease with which random signals can be generated. Band-limited Gaussian white noise can be easily generated by amplifying the potential across a Zener diode. Ideally, white noise has a power spectrum which is constant for all frequencies. The diode power spectrum in reality is bandwidth-limited and thus the random noise can be thought of as bandwidth-limited white noise. Fig. 4 illustrates a home-built circuit used to obtain Gaussian noise for load simulation.

2.4 Track-Hold Noise

Because the Zener diode noise contains very high frequencies, the OPAMPs in the analog computer register overloading during integration. A technique used to remedy this problem is to first process the noise through a track-hold circuit. The track-hold circuit is designed such that the noise is tracked when a control voltage is positive, and the last sampled noise voltage is held constant when the control voltage is negative. By allowing the control voltage to periodically jump from positive to negative, a track-hold circuit is obtained which can hold the noise for a short time, sample the signal, hold the new value and so on. The noise sampling frequency is determined by the control voltage frequency. The resulting track-hold signal is a series of randomly occurring, short straight lines of uniform length (Fig. 5). The track-hold signal was tested

to insure that the Gaussian distribution of the noise generator was not altered by the track-hold circuit.

For the present, the Gaussian signal $x(t)$ from the Zener diode will be called $\Delta\sigma(t)$ for illustrative purposes. The structural stress due to gust loading $\sigma(t)$ can be fitted to a Gaussian distribution, but that is not the same as $\Delta\sigma(t)$, which is the peak-to-peak amplitude difference for a fatigue cycle. The essence of the Monte Carlo method is that its development is not dependent on the assumed $\Delta\sigma(t)$ distribution, which is taken to be Gaussian for convenience.

It is convenient to let the computer determine the mean and standard deviation of the random load as a check to insure that the proper load distribution has been modeled. Since the loading signal is known to be Gaussian, all that is necessary to describe the distribution is the mean and first moment. For continuous functions, the mean and variance are given approximately by:

$$\mu = \frac{1}{T} \int_0^T x(t) dt \quad \sigma^2 = \frac{1}{T} \left\{ \int_0^T x^2(t) dt - \frac{1}{T} \left[\int_0^T x(t) dt \right]^2 \right\} \quad (8)$$

The symbolic program for these circuits is shown in Fig. 6. Computing the mean and standard deviation over a finite time interval is only valid when the $\Delta\sigma(t)$ is an ergodic stationary random process. Ergodic stationary processes are those for which each ensemble record is statistically equivalent to all other records and for which ensemble averages can be replaced by time averages of a single record. The limit of the time average over a finite interval from time 0 to T, as T tends to infinity, will be equivalent to the ensemble average for ergodic processes.

The track-hold circuit serves two purposes. First, periodic sampling and holding of the continuous Gaussian noise is needed to reduce the high overload frequencies to a level which the analog circuitry can tolerate. Second, the resulting blocks of $\Delta\sigma$ make digital program verification convenient with regard to the load description.

Inaccuracies of the crack size distribution will result from insufficient sampling of the loading. For more realistic load modeling, the track-hold circuitry would not be used and either more expensive analog circuitry with wider frequency characteristics or frequency filtering of the signal would be necessary.

2.5 Paris Solution for Random Loading

Solving the Paris growth equation with random loading becomes a simple matter once the appropriate material constants and load distribution statistics are determined. A symbolic diagram of the analog program appears in Fig. 7. The solution of the growth equation actually takes very few components compared to the load generation and statistical circuits. Fig. 8 illustrates a growth solution in real time for an initial crack of 0.1 inch subjected to random loading with a mean of 37 ksi and standard deviation of 3.9 ksi for 15,000 cycles. The time average and standard deviation of the loading are computed over a 10 second interval. With the load history recorded and inserted into the digital CRACKS II program, a solution

which can be considered exact verifies the accuracy of the analog solution. This check is done to insure that the rapid changes in the loading during the track-hold sample mode are not disturbing the analog circuitry. It is now apparent that the time scaling can be altered such that much faster computing is available, provided that solution accuracy is retained.

2.6 Repetitive Operation (REPOP)

High speed analog computers have the capability of repeating a problem solution by use of the repetitive operation (REPOP) mode. This condition provides a means of switching the integrators between the reset (initial condition) and the operate (integration) modes. The TR-48 10-mfd integrator feedback capacitors are replaced with 0.02-mfd capacitors to change the problem time scale by a factor of 500. Normally the REPOP mode is used primarily for sweeping oscilloscope output. However, for solutions in the 400 to 500 millisecond range, the REPOP mode can be used with chart recording equipment. The REPOP mode permits the calculation of several hundred problems in a very short time.

With such a decrease in solution time, there exist cases where crack growth or response is so rapid that errors are induced in the OPAMPs as well as in the chart recorder. A sample problem was run as before, but in the REPOP mode for an accuracy check. Fig. 9 illustrates the output from the problem solution. By recording the load history and repeating the problem on CRACKS II, two solutions were obtained, one for $a_0 = 0.110$ inch and one for $a_0 = 0.112$ inch.

Since it is difficult to read the analog a_0 to a third significant figure, the two digital solutions were computed and found to bound the analog solution within the output tolerances. Note how the solution accuracy deteriorates with a relatively small error in the initial crack size. The exponential nature of the growth solutions demands careful attention when using analog circuitry, since overloading may occur without much disturbance. The above REPOP solution simulated crack growth over 20,000 fatigue cycles lasting 0.40 seconds, or with a time scaling of 1 second equal to 50,000 fatigue cycles. For a series of 200 problems assuming 20,000 cycles each and 0.50 seconds for each problem including reset time, the entire run would last 100 seconds.

2.7 Errors and Special Circuitry

Due to the nature of the family of crack growth solutions, several sources of error are present. Perhaps the most significant is the potential range and frequency of the exponential solutions occurring in less than one-half second of computation time. Because the growth rates are functions of the loading $\Delta\sigma^4(t)$, there exist cases where the loads will become large enough during the problem solution time for crack sizes to grow rapidly by several orders of magnitude. This presents a difficult problem for analog computers since their variable range is only one order of magnitude, or, at most, two. However, it is possible to reduce this problem by rescaling variables internally in the program. For example, in problems where initial flaw sizes are 0[0.005 inch] and the solution

time and loads are such that cracks could grow to 0[0.07 inch], the growth equation solutions can be divided into two problems:

1. A variable scaling of 1.0 machine volt equal to 0.001 inch.
2. A rescaling of 1.0 machine volt equal to 0.01 inch when the crack grows to 0.01 inch or larger.

If the entire two-magnitude range is attempted in the scaling of 1 volt equal to 0.01 inch, the initial flaw value must be less than 1 volt. Beginning the solution at such a small voltage, especially for an exponential solution, taxes the tolerance limits of the analog accuracy over the 10-volt range. Observing the solutions on an oscilloscope, it is quite easy to see the accumulation of errors at an initial crack voltage level of, say, 0.5 volts by observing apparent growth for no loading. More modern and sophisticated analog computers can have a variable range of ± 100 volts, which greatly reduces the problems of two-magnitude solution ranges. However, for this study, the TR-48 has a ± 10 volt range and special circuitry or programming is required.

The design of circuitry to consider both small and large cracks is based on the availability of logic flip-flops or electronic switches controlled by signal comparators. The flip-flops are solenoid-controlled switches which have a propagation time of several milliseconds and should be avoided if possible, since they are not entirely reliable. Electronic switching devices are much more expensive but are worth the extra cost since they are quite fast (propagation time approximately 5 microseconds). A logic circuit can be devised with electronic switches such that when the

crack size is below, say, 0.01 inch, the first growth circuit for small cracks is integrating and the second circuit for large cracks is in stand-by in the reset mode until the crack grows to 0.01 inch. Then, with appropriate switching, the first circuit is taken out to prevent overloading and is replaced by the rescaled second circuit with an initial condition of 0.01 inch and allowed to continue integrating the solution for the remaining computing time. A third stage can be added if required, or an overload prevention switch can be used to prevent growth beyond 10 volts (0.1 inch) in the new rescaled circuit.

In the REPOP Monte Carlo program, caution must be taken to prevent OPAMP overloading or saturation with voltages greater than 10 volts, since a few seconds are required to unsaturate the amplifiers. When using loads with a large variance, many solutions might overload the circuitry requiring shut-down and relaxation time before continuing.

In addition to variable errors, inaccuracies in REPOP computing time are also significant. Figure 10 shows the REPOP solution of a typical problem in which $\Delta\sigma$ is constant. The chart speed has been reduced to show several problems. Since $\Delta\sigma$ is constant, the computer is solving the same problem repeatedly, but the final solution values are not consistent. Due to slight variations in the REPOP resetting and operating switches, the exponential solutions exhibit variance due to microsecond propagation-time errors in the switches. Proper care must be taken to insure constant solution time. When chart recording equipment is used, each solution

must be recorded by hand. In the case of digital sampling equipment, care is needed to make sure that identical solutions are recorded for constant loading.

2.8 Sample Monte Carlo Run

With the program used in Fig. 11 patched into the analog computer and a constant $\Delta\sigma$ test solution made to insure correct material constant settings, a sample Monte Carlo run was made for 250 problems. The initial crack size remained constant at 0.1 inch with a maximum allowed solution of 1.0 inch. Using typical Paris constants for aluminum and Gaussian loading with a 26.7 ksi mean and 7.5 ksi standard deviation, crack growth distributions were recorded at 10,000, 15,000, and 20,000 fatigue cycles as given in Figs. 12 through 14. Because the range of solutions was well within one magnitude, no special switching and rescaling circuitry was required. As expected, the distributions shift and spread out with increased fatigue.

Section 3

EXTENDED MONTE CARLO SIMULATION

An extended Monte Carlo simulation of the Paris equation was conducted to generate an example data base for final crack size, in order to illustrate the use of the Monte Carlo method in risk analysis. Typical properties for 0.09-inch thick 7075-T6 aluminum sheet [5] were used to define the Paris equation constants and a critical crack size. The following Gaussian distribution for stress range $\Delta\sigma$ was assumed:

$$f(\Delta\sigma) = \frac{1}{8.25\sqrt{2\pi}} \exp \left\{ -\frac{1}{2} \left(\frac{\Delta\sigma - 14.25}{8.25} \right)^2 \right\} \quad (9)$$

where $\Delta\sigma$ is in units of ksi. The simulation was repeated for eleven initial crack sizes ranging from 0.005 to 0.07 inch. The objective of the simulation was defined to be production of a final crack size histogram, corresponding to each assumed initial crack size, after growth computation over 20,000 load cycles, which simulated approximately 4,000 flight hours. In addition, it was hoped that this amount of growth would result in significant probabilities for achieving final crack sizes greater than the critical size. The simulation achieved the latter objective partially.

3.1 The Computation Problem and Its Solution

The Paris equation for crack growth may be integrated to the form:

$$a_i^{1-N_p/2} - a_f^{1-N_p/2} \approx \left(\frac{N_p}{2} - 1 \right) C_p \int_0^N (\Delta\sigma)^{N_p} dN \quad (10)$$

where a_i is any given initial crack size, and where a_f represents the corresponding final crack size after N fatigue cycles. If a risk analysis of initial flaw size variability is intended, a_i is the independent random variable in Eq. 10, and the distribution for a_f can be derived in the following simple manner. Since the load history $\Delta\sigma$ is deterministic for the purpose of the analysis, Eq. 10 represents a one-to-one relationship between a_i and a_f values. Furthermore, the right-hand side of Eq. 10 is positive so that for any two a_i values:

$$a_{f2} > a_{f1} \text{ if and only if } a_{i2} > a_{i1} \quad (11)$$

In other words, the solutions do not cross over as N is varied, and therefore:

$$F_f(a_f|a_i, N) = F_i(a_i) \quad (12)$$

where

$$F_f(a_f|a_i, N) = \Pr\{\text{Final Crack Size} \leq a_f, \text{ given } a_i, N\} \quad (13)$$

$$F_i(a_i) = \Pr\{\text{Initial Crack Size} \leq a_i\} \quad (14)$$

Hence, the final crack size distribution may be determined with reasonable accuracy by repeating the growth computation (Eq. 10) for 10 to 20 a_i values.

The above direct procedure is made possible by the explicit relation between the dependent and independent random variables a_f and a_i . However, the implicit relationship between a_f and $\Delta\sigma$ prevents the inference of a simple analytical correspondence similar

to Eqs. 11 and 12. Also, an appeal to the central limit theorem of probability theory offers only a crude approximation by considering a_f as the sum of a large number of uncorrelated random variables. It is therefore necessary to conduct a Monte Carlo experiment to determine F_f where service loading is the independent random variable. If no a priori assumptions are made about the form of the final crack size distribution, 200 to 300 replicate computations are required to obtain a good experimental histogram [2], and 2,000 to 3,000 computations are required to study 10 selected a_i values. This heavy digital computing burden is increased further if one attempts to have the load history simulate reality more closely by increased fineness in layering, i.e., by assigning fewer load cycles per block and increasing the randomization of block sequence.

Analog computation was therefore examined and developed as an alternate scheme for crack growth calculation in the present program. A brief review of the analog scaling requirements as they pertain to the relations between computing time, number of events, and equivalent flight hours is given here to provide a complete picture of the data base generation technique. The following factors constitute of set of constraints on the Monte Carlo experiment, within which a realistic operating point must be found.

First, efficient use of the analog computer for several hundred or more runs requires employment of the repetitive operation mode, in which each run consumes on the order of 0.5 second in real time. Of this total, roughly 0.4 second is spent on computation and 0.1 second is required as reset time for the next run. The real time

consumed for computation should correspond to the total number of load ($\Delta\sigma$) events expected in one service life.

Second, the load history is simulated by a random noise generator and track-hold circuit which produce a nearly square-wave signal for $\Delta\sigma$. Each level portion of the signal is of constant duration (controlled by the track-hold frequency) and may be identified as a load block representing a number of fatigue cycles at constant stress range. The achievement of a realistic simulation requires some care in the choice of track-hold frequency. At one extreme, a very wide dispersion in a_f values results if the track-hold frequency is very low. This extreme tends toward an experiment in which constant-amplitude fatigue is simulated, with the choice of range being a random variable at the beginning of each run. This is obviously completely unrepresentative of fleet service experience. At the other extreme, the random noise signal may be input directly, without benefit of the track-hold filter. This is desirable from a simulation viewpoint, but the high-frequency components of the signal tend to overload the analog integrating circuits, thus making the results of questionable validity. Hence, a minimum track-hold frequency must be chosen, such that at least a few hundred samples of the random noise are obtained during each run to insure adequate sampling of the stress range distribution.

Combination of the above requirements defines the relationships between computing time, service life and load blocking. In the present case, the time scaling:

$$N = 50,000 \text{ t} \quad (15)$$

was chosen. According to Eq. 15, a 0.4-second computing time is equivalent to 20,000 events or approximately 3,560 flight hours. This time scaling was chosen to achieve a reasonable simulation of one airplane service life.

Preliminary experiments with track-hold frequency indicated that the dispersion of final crack size values changed very little for frequencies between 200 and 1,200 Hz. The track-hold frequency was set at 500 Hz for the Monte Carlo experiment; i.e.,

$$500 \text{ Hz} \times 0.4 \text{ sec} = 200 \text{ samples per run} \quad (16)$$

$$\frac{50,000 \text{ events/sec}}{500 \text{ Hz}} = 100 \text{ events per block} \quad (17)$$

3.2 Description of the Monte Carlo Simulation

The objective of the Monte Carlo simulation was to grow small initial flaws ($0.005 \text{ inch} \leq a_i \leq 0.07 \text{ inch}$) to final sizes of the order of the critical crack size (0.122 inch). This objective was achieved for initial flaws in the range $0.03 \leq a_i \leq 0.07 \text{ inch}$. However, the amount of growth observed for very small flaws ($0.005 \leq a_i \leq 0.01 \text{ inch}$) was insignificant under the given load spectrum.

Approximately 200 replicate runs were made for each a_i value. The analog output of crack size as a function of time was recorded on a strip chart recorder. Subsequently, templates were used to read the crack size at four points on each run, corresponding to:

$$N = 8,000, 10,000, 13,300, 20,000 \text{ events} \quad (18)$$

The crack size data were then keypunched and processed on a digital computer to produce observed data histograms and to estimate parameters for various trial distributions. Data histograms for final

crack sizes grown from $0.03 \leq a_i \leq 0.07$ inch are shown in Figs. 15 through 33.

The three-parameter Weibull distribution:

$$f(x) = \frac{\alpha(x-x_0)^{\alpha-1}}{\beta^\alpha} e^{-\left(\frac{x-x_0}{\beta}\right)^\alpha} \quad F(x) = 1 - e^{-\left(\frac{x-x_0}{\beta}\right)^\alpha}; \quad \alpha, \beta > 0 \quad x \geq x_0 \quad (19)$$

was used to correlate the results. The initial flaw size is a logical choice for the lower-bound parameter x_0 in the present case. Hence, the model becomes:

$$F_f(a_f | a_i, \nu) = 1 - e^{-\left(\frac{a_f - a_i}{\beta}\right)^\alpha} \quad (20)$$

where α, β may be functions of a_i and ν , and where

$$\nu = N/20,000 \quad (21)$$

defines the fraction of service. The crack size data thus correspond to (see Eq. 18):

$$\nu = 0.4, 0.5, 0.667, 1 \quad (22)$$

Note that $\nu = 1$ is equivalent to 3,560 flight hours.

The following maximum likelihood estimator formulas for α, β may be derived easily for the three-parameter Weibull family under the assumption that the lower-bound parameter is known:

$$\hat{\alpha} = \frac{N \sum_{j=1}^N (x_j - x_0)^{\hat{\alpha}}}{N \sum_{j=1}^N (x_j - x_0)^{\hat{\alpha}} \ln(x_j - x_0) - \left[\sum_{j=1}^N (x_j - x_0)^{\hat{\alpha}} \right] \left[\sum_{j=1}^N \ln(x_j - x_0) \right]} \quad (23)$$

$$\hat{\beta} = \left[\frac{1}{N} \sum_{j=1}^N (x_j - x_0)^{\hat{\alpha}} \right]^{1/\hat{\alpha}} \quad (24)$$

where x_1, x_2, \dots, x_N are the observed data. Equation 23 may be solved for $\hat{\alpha}$ by iteration, after which $\hat{\beta}$ is obtained explicitly from Eq. 24. Tables 3 and 4 summarize the estimates thus obtained for $\hat{\alpha}$ and $\hat{\beta}$, respectively, by digital processing of the raw data. The case of $a_i = 0.06$ inch (60 mils) and $v = 1$ is an exception, the analog data having been accidentally lost. The scale parameter $\hat{\beta}$ for this case was estimated subsequently from the empirical correlation discussed below.

In seeking to correlate the results for $\hat{\alpha}$ and $\hat{\beta}$, one must make some approximate hypothesis which can be followed analytically to a conclusion which will provide a guide. One possible hypothesis is to ignore temporarily the random nature of $\Delta\sigma$, allowing analytical integration of Eq. 10 to the form:

$$\Delta\sigma \sim \left[\frac{a_f - a_i}{c_p N a_f a_i} \right]^{1/4} \quad (25)$$

for $N_p = 4$. If this hypothesis is combined with the further assumption that

$$\Pr\{\text{Final Crack Size} \leq a_f\} \sim \Pr\{\text{Load} \leq \Delta\sigma\} \quad (26)$$

and $\Delta\sigma$ is modeled with a Weibull distribution,

$$F(\Delta\sigma) = 1 - e^{-\left(\Delta\sigma/\hat{B}\right)^{\hat{A}}} \quad (27)$$

there results:

$$F_f(a_f | a_i, v) \sim F(\Delta\sigma) = 1 - \exp \left\{ - \left[\frac{a_f - a_i}{c_p \hat{\beta}^4 N a_f a_i} \right]^{\hat{A}/4} \right\} \quad (28)$$

Finally, assuming that $a_f a_i \sim a_i^2$ and replacing $C_p \hat{B}^4 N$ by $C v$, where C is an appropriate constant, leads to:

$$F_f(a_f | a_i, v) \sim 1 - e^{-\left(\frac{a_f - a_i}{\hat{\beta}}\right)^{\hat{\alpha}}} \quad (29)$$

$$\hat{\alpha} = \hat{A}/4, \quad \hat{\beta} = C v a_i^2$$

In other words, the shape parameter for the final crack size model ought to be about one-fourth of the estimated loading shape parameter, and the final crack size scale parameter should correlate with $v a_i^2$. One would expect this chain of argument to hold rigorously for constant-amplitude fatigue with randomly chosen amplitude, and one might apply it approximately if most of the crack growth were confined to the last few load cycles. However, its utility in the present case is limited to the function of a general guide.

Since the foregoing argument indicates that a constant $\hat{\alpha}$ is expected for final crack size when the load spectrum is kept constant, mean and standard deviation were estimated for $\hat{\alpha}$ from the data in Table 3, with the results:

$$\hat{\mu}_{\hat{\alpha}} = 1.48 \quad \hat{\sigma}_{\hat{\alpha}} = 0.289 \quad (30)$$

These results may be compared with the load distribution by means of the well-known relationship:

$$\alpha \approx \mu/\sigma \quad ; \quad \alpha > 1 \quad (31)$$

Applying Eq. 31 to Eq. 9, we find:

$$\hat{A} \approx 14.25/8.25 = 1.73 \quad (32)$$

Comparison of Eqs. 30 and 32 shows that the estimated mean for $\hat{\alpha}$ is less than but within one standard deviation of \hat{A} . We may

therefore conclude tentatively that the variability of the service load distribution is impressed more or less directly on the final crack size distribution.

The final crack size scale parameters $\hat{\beta}$ in Table 4 were subjected to separate regression analyses with respect to ν and a_i . These analyses indicated that:

$$\hat{\beta} \sim (\nu a_i^2)^{1.2} \quad (33)$$

The final correlation for $\hat{\beta}$ is illustrated in Fig. 34. The correlation line shown in the figure was fit by eye and gives:

$$\hat{\beta} \cong 2.34 \times 10^{-3} (\nu a_i^2)^{1.2} \quad (34)$$

with a_i in units of mils.

The foregoing results show that the approximate hypothesis based on a fully integrated growth equation does indeed provide only a general guide. The correlation for $\hat{\beta}$ is in general agreement with the hypothetical model. However, much less broadening of the final crack size distributions, relative to the load distribution, is observed in comparison with the prediction of the hypothetical model. For the purpose of further analysis, the final crack size distribution may be taken as:

$$F_f(a_f | a_i, \nu) = 1 - \exp \left\{ - \left[\frac{a_f - a_i}{2.34 \times 10^{-3} (\nu a_i^2)^{1.2}} \right]^{1.48} \right\} \quad (35)$$

However, no special significance should be attached to Eq. 35. It is merely the result of an empirical correlation, and is useful only for interpolation within and near the ranges of initial flaw size a_i and service fraction ν over which the Monte Carlo experiments were conducted.

3.3 Risk Sensitivity Assessment

The risk for a crack to exceed critical size due to the combined effects of random loading and a random initial flaw population may be assessed by combining the results of the Monte Carlo experiment with a description of the initial flaw distribution. Since it is logical to assume that the random variables a_i and $\Delta\sigma$ are uncorrelated, the following simple procedure may be used to compute mathematical risks:

$$\bar{R}_f(a_{cr} | \nu) = \int_0^{\infty} R_f(a_{cr} | a_i, \nu) f_i(a_i) da_i \quad (36)$$

where \bar{R}_f represents the risk of exceeding a_{cr} , given the service fraction ν , and where:

$$R_f(a_{cr} | a_i, \nu) = 1 - F_f(a_{cr} | a_i, \nu) = \exp \left\{ - \left(\frac{a_{cr} - a_i}{\beta} \right)^{\hat{\alpha}} \right\} \quad (37)$$

$$f_i(a_i) da_i = \text{Pr} \{ a_i \leq \text{Initial flaw size} \leq a_i + da_i \} \quad (38)$$

Approximate risk assessments may be made by computing $R_f(a_{cr} | a_i, \nu)$ at a few equally-spaced a_i values and using the trapezoid rule:

$$\bar{R}_f(a_{cr} | \nu) \approx \sum_j R_f(a_{cr} | j \Delta a, \nu) f_i(j \Delta a) \Delta a \quad (39)$$

together with the assumption that $R_f(a_{cr} | 0, \nu) = 0$.

The initial flaw distribution referred to in Eqs. 36, 38, and 39 must be defined to correspond to the flaw population which may escape into the structure at the beginning of service. Models for

this population may be constructed by combining data on the distribution of flaws created by materials processing and machining with data on inspection reliability. Let $f_{mfg}(a_i)$ be the probability density function which characterizes the "as-manufactured" flaw population, and suppose that nondestructive inspection (NDI) data are available in the form of a detection probability curve:

$$P_d(a) = \Pr\{\text{Initial flaws } \geq a \text{ are detected by NDI}\} \quad (40)$$

Some typical detection probability curves are shown in Fig. 35. Since the events of flaw creation and detection or escape may reasonably be assumed to be uncorrelated, the initial flaw distribution in service may be computed from:

$$f_i(a_i) = \frac{[1 - P_d(a_i)] f_{mfg}(a_i)}{\int_0^{\infty} [1 - P_d(a)] f_{mfg}(a) da} \quad (41)$$

The effect of Eq. 41 is illustrated schematically in Fig. 36, while Fig. 37 outlines the procedure for computation of the mathematical risks associated with exceedance of critical crack size. Since there are commonly no data available for estimation of $f_{mfg}(a)$, good statistical practice dictates that the creation of flaws of any size be assumed equally likely up to some maximum size so large that the risk of escape from detection is negligible. In this case, Eq. 41 is replaced with:

$$f_{mfg}(a) = 1/a_{max} \quad ; \quad 0 \leq a_i \leq a_{max} \quad (42)$$

$$f_i(a_i) \cong \frac{[1 - P_d(a_i)]^{1/a_{max}}}{\int_0^{a_{max}} [1 - P_d(a)] da / a_{max}} \cong \frac{1 - P_d(a_i)}{\int_0^{\infty} [1 - P_d(a)] da} \quad (43)$$

An example risk sensitivity assessment has been carried out using the critical crack size exceedance function $R_f(a_f|a_i, v)$ obtained from the Monte Carlo simulation in combination with several possible assumptions about the initial flaw distribution and inspection procedures. Table 5 summarizes the critical crack exceedance risks for a matrix of service fractions v and assumed initial crack sizes a_i . The results in this table include extrapolation outside the a_i range over which the simulation was conducted. In Table 6, the details of the computation summarized by Eq. 39 are shown, using the equal-likelihood hypothesis for "as-manufactured" initial flaws (Eqs. 42 and 43) and the "Mechanized Probe" detection probability curve from Fig. 35. The summations in this table are risks associated with equal-likelihood as-manufactured flaws, mechanized-probe NDI, and a hypothetical proof test which positively rejects any initial flaw larger than 100 mils. To obtain the corresponding risks for NDI only, one need simply observe that $R_f(a_{cr}|a_i, v) \approx 1$ for $a_i > 100$ mils. Hence, the case of NDI only may be computed by adding the quantity

$$1 - F_i(100 \text{ mils}) = 0.0428 \quad (44)$$

to the summations in Table 6.

It is interesting to compare the mathematical risks described above with a parallel assessment in which sensitivity to the initial flaw population is retained, while random loading effects are ignored. Since the random process adopted for the above examples was simply a Gaussian-distributed stress range, one possible measure for the corresponding deterministic loading process is constant-amplitude

fatigue at the spectrum mean stress range (14.25 ksi). This is referred to as "central loading" for convenience. In this case, the Paris equation may be integrated to:

$$a_f = \left[\frac{1}{a_i} - 3.22 \nu \right]^{-1} \quad (45)$$

where a_f and a_i are in units of inches. The results of this calculation are summarized in Table 7. Critical crack exceedance risks for the case of central loading may be computed as follows. For a given service fraction ν , determine by interpolation from Table 7 the $a_{i_{cr}}$ value for which $a_f = a_{cr} = 122$ mils. The risk is then given by $1 - F_i(a_{i_{cr}})$.

Finally, three additional cases have been included, in which some hypothetical assumptions have been made about the as-manufactured flaw population and for which NDI without a proof test has been assumed. Hypothetical Gaussian distributions:

$$f_{mf_g}(a) = \frac{1}{\sigma\sqrt{2\pi}} \exp \left\{ -\frac{1}{2} \left(\frac{a-50}{\sigma} \right)^2 \right\} \quad (46)$$

were assumed, with a in units of mils, and with $\sigma = 10, 15, 20$ mils. These distributions thus have coefficients of variation of 0.2, 0.3, 0.4 respectively. Table 8 summarizes the as-manufactured probability densities and the initial flaw probability densities computed from Eq. 41. Combined risk calculations have been carried out for each of these distributions, as shown in Tables 9, 10, and 11.

Table 12 gives a comparative summary of the mathematical risks computed for each of the cases described above. The first two lines in this table assume an equal-likelihood manufactured population and

account for random loading. The third and fourth lines correspond to deterministic-load risk assessment with the same initial populations. The last three lines account for randomness in the loading and the initial flaw population, and are intended to illustrate the sensitivity of risk to dispersion in the initial population.

The mathematical probabilities in Table 12 present quite different pictures of the risk of achieving a critical crack size. At one extreme, two models predict small or no risk at short service times, with the risk function rising rapidly as the service approaches one life. These two extreme models are the central load calculation with equal-likelihood initial population filtered by NDI and proof test, and the random load calculation with Gaussian initial population ($CV = 0.2$) filtered by NDI. At the other extreme, two models predict rather high risk over the entire service period considered, with the risk function relatively insensitive to service time. These are the random load calculation with equal-likelihood initial population filtered by NDI, and the corresponding central load calculation. The other cases are seen to give risk functions which lie between these extremes.

It is apparent from these results that the procedures which might be adopted to minimize risks for service times less than one life depend strongly upon which model is accepted as a true description of nature. Thus, if the equal-likelihood population is assumed for manufactured flaws and random load is accounted for, one is led to strategies of either a proof test to reject initial flaws much smaller than 100 mils or development of some NDI method which will

give better detection probabilities. On the other hand, the given NDI method supplemented by the 100-mil proof test appears to be a good strategy if the effects of random loading are ignored. Of course, the equal-likelihood manufactured flaw population is a very conservative assumption, even though accepted statistical practice demands it in the absence of experimental data. The examples with Gaussian manufactured populations demonstrate that it may be worthwhile to obtain enough data to determine at least approximately the coefficient of variation for as-manufactured flaw populations. Finally, it is interesting to compare these latter cases directly with the data in Table 5. Each line in Table 5 may be treated as a risk function which corresponds to an assumption that all initial flaws have a common deterministic size, a view which is convenient for design calculations. The question is whether it is possible to choose a flaw size which leads to a risk function with behavior similar to the risk functions based on the entire flaw population. In the present case, the answer is affirmative if $a_i \approx 70$ mils is chosen for short times and $a_i \approx 55$ mils is chosen for service periods approaching one life.

Section 4

DISCUSSION AND CONCLUSIONS

Results have been presented for a fatigue crack growth risk analysis for which a Gaussian stress range spectrum was assumed, and for which a critical crack size for fracture was estimated approximately as 0.122 inch in 7075-T6 aluminum alloy. The stress range spectrum was found to be capable of growing cracks from initial sizes between 0.03 and 0.07 inch to the critical crack size after 20,000 stress range events, a total which corresponds to approximately 3,600 flight hours.

The objective of the analysis was to generate a data base for final crack size at several fractions of service, from which the risks of structural failure could be assessed. The risk study focussed primarily on the contribution of dispersion in the load spectrum to the dispersion of final crack sizes. Average service experience for a fleet, when translated into a final crack size, provides only limited information about fleet safety. The calculation of failure rates requires crack growth computations for non-representative as well as average service history within a given mission spectrum. Since no analytical derivation can be given for the distribution of final crack sizes as a function of the stress range distribution, a Monte Carlo simulation is required, in which a crack growth rate equation is integrated several hundred times from the same initial crack size. A technique of analog computer

simulation was developed and verified for this purpose. The analog method was shown to be cost-effective for extended Monte Carlo simulations, in comparison to digital computation. Also, the stress range spectrum was shown to be easily representable by input of a filtered signal from a random noise generator. The random noise signal automatically provides a series of load histories with controlled parameters which fit the given mission spectrum (stress range mean and standard deviation) as the analog repeatedly integrates the crack growth rate equation. With the analog set in repetitive operation, approximately 30 minutes were required to generate 200 curves of crack size versus equivalent flight hours for each of 11 assumed initial crack sizes. Four data points were sampled from each curve (0.4, 0.5, 2/3 and full service period) and were processed digitally to provide histograms for final crack size, with time and initial size as parameters. The raw data histograms for five initial sizes are presented in this report.

The three-parameter Weibull distribution was chosen as a logical model for the probability distribution for final crack size. With the lower-bound location parameter assumed equal to the initial crack size for each histogram, the analog data were used to compute maximum likelihood estimates for the scale and shape parameters. A regression analysis of the scale parameters resulted in good empirical correlations with $(va_i^2)^{1.2}$, where v represents service fraction and a_i is the initial crack size. These results agreed generally with an approximate estimate which predicted va_i^2 for the correlation. The approximate estimate also predicted a final crack size dispersion

of four times the load spectrum dispersion. However, the final crack size shape parameters estimated from the analog data indicated that the dispersion of final crack size is only slightly greater than the load dispersion. Shape parameters for final crack size were therefore defined accordingly, and were used together with the empirical correlations for scale parameter to extrapolate the data base to a few near-neighboring initial crack sizes which had not been included in the simulation.

The final crack size data base was used to compute the mathematical risks of exceeding the critical crack size, as a function of service time, for several sets of assumptions about initial flaw populations and manufacturing quality-control strategies. For the parameters considered in the present study, the results indicated that risk functions based on deterministic assumed initial flaw sizes between 55 and 70 mils were similar to the risk functions based on assumed flaw populations with a mean size of 50 mils and coefficients of variation between 0.2 and 0.4 which were subjected to filtering by nondestructive inspection. Risk functions were also computed for cases which considered a flaw population but neglected random load effects. These risk functions were observed to behave quite differently from those calculated for corresponding cases which included the effects of random loading. This comparison may have a significant bearing on risk assessments of aircraft which are fatigued primarily by gust loading, but must be considered much less important for aircraft which are fatigued primarily by quasi-deterministic maneuver loads.

There appears to be no reason why the analog method cannot be extended to more sophisticated simulations, in which the effects of stress ratio, retardation, multiple sources of random loading, ground-air-ground cycles, etc., are included. The feasibility of such extensions depends, of course, upon the availability of a sufficient amount of analog hardware, and upon calibration by parallel digital analysis to verify computational accuracy. Given these conditions, the most useful application of the analog approach to crack growth simulation appears to be rapid assessment of the sensitivity of fleet risk functions to changes in load spectra.

REFERENCES

1. Engle, R. M., "CRACKS, A Fortran IV Digital Computer Program for Crack Propagation Analysis," AFFDL-TR-70-107, 1970.
2. Hahn, G. J. and Shapiro, S., Statistical Models in Engineering, John Wiley, New York, 1968.
3. Liebowitz, H., Fracture, Vol. III, Ch. 1, Academic Press, New York, 1971.
4. Tomovic, R. and Karplus, W. J., High Speed Analog Computers, Dover, New York, 1962.
5. Damage Tolerant Design Handbook, Air Force Flight Dynamics Laboratory, Wright Patterson, Ohio, September 1973.

TABLE 1
COMMON LINEAR ANALOG COMPONENTS

SIMPLE CIRCUITS USING AMPLIFIERS AND POTENTIOMETERS

CIRCUIT DESCRIPTION	CIRCUIT	COMPUTER SYMBOL
1. GROUNDED POTENTIOMETER		
2. UNGROUNDED POTENTIOMETER		
3. INVERTER		
4. MULTIPLICATION BY -10		
5. MULTIPLICATION BY -k for $1 \leq k \leq 10$ (for $k < 1$ use circuit 1 feeding circuit 3.)		
6. MULTIPLICATION BY 2		
7. MULTIPLICATION BY $\frac{1}{2}$		

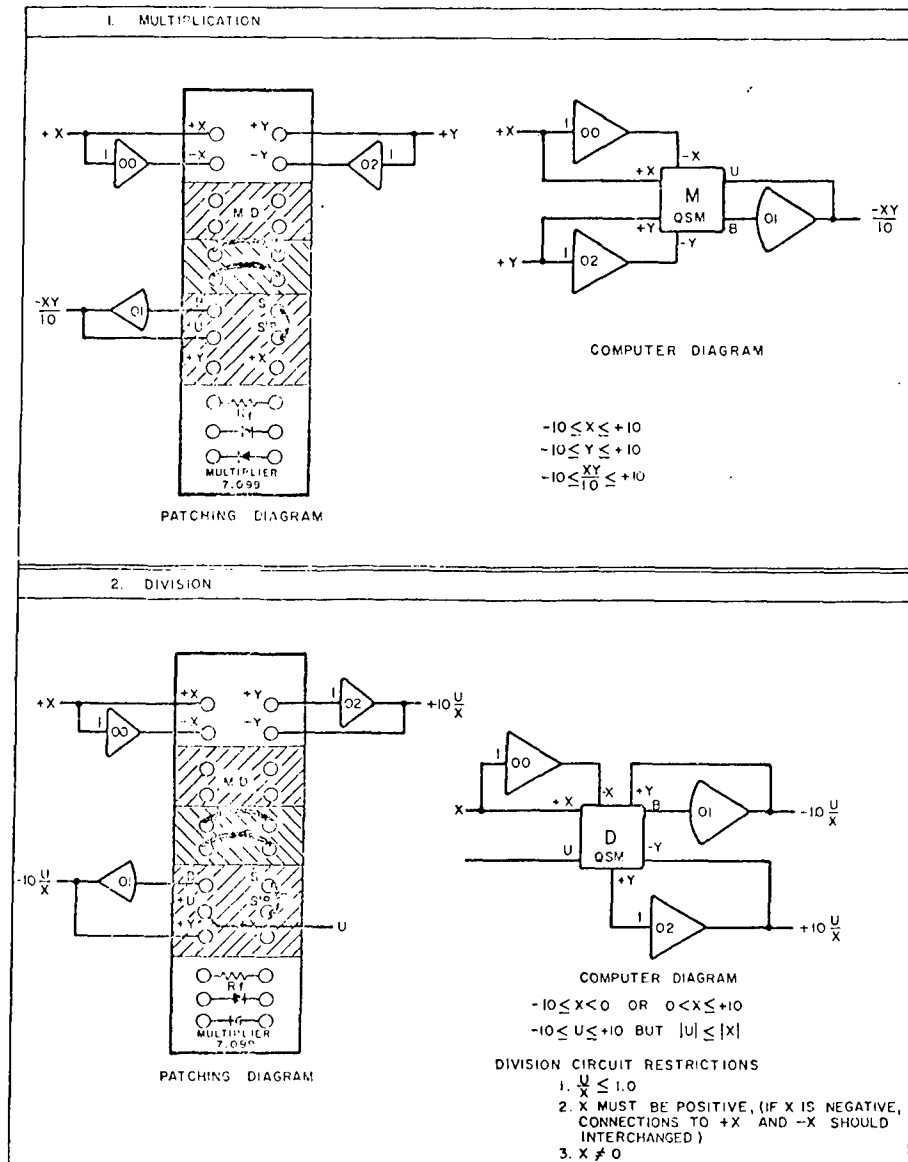
Courtesy of EAI-TR-48 Reference Guide

CIRCUIT DESCRIPTION	CIRCUIT	COMPUTER SYMBOL
8 MULTIPLICATION BY $\frac{1}{10}$		
9. MULTIPLICATION BY AN ARBITRARY VALUE		
10. ADDITION		
11. SUBTRACTION		
12 INTEGRATION		

Courtesy of EAI-TR-48 Reference Guide

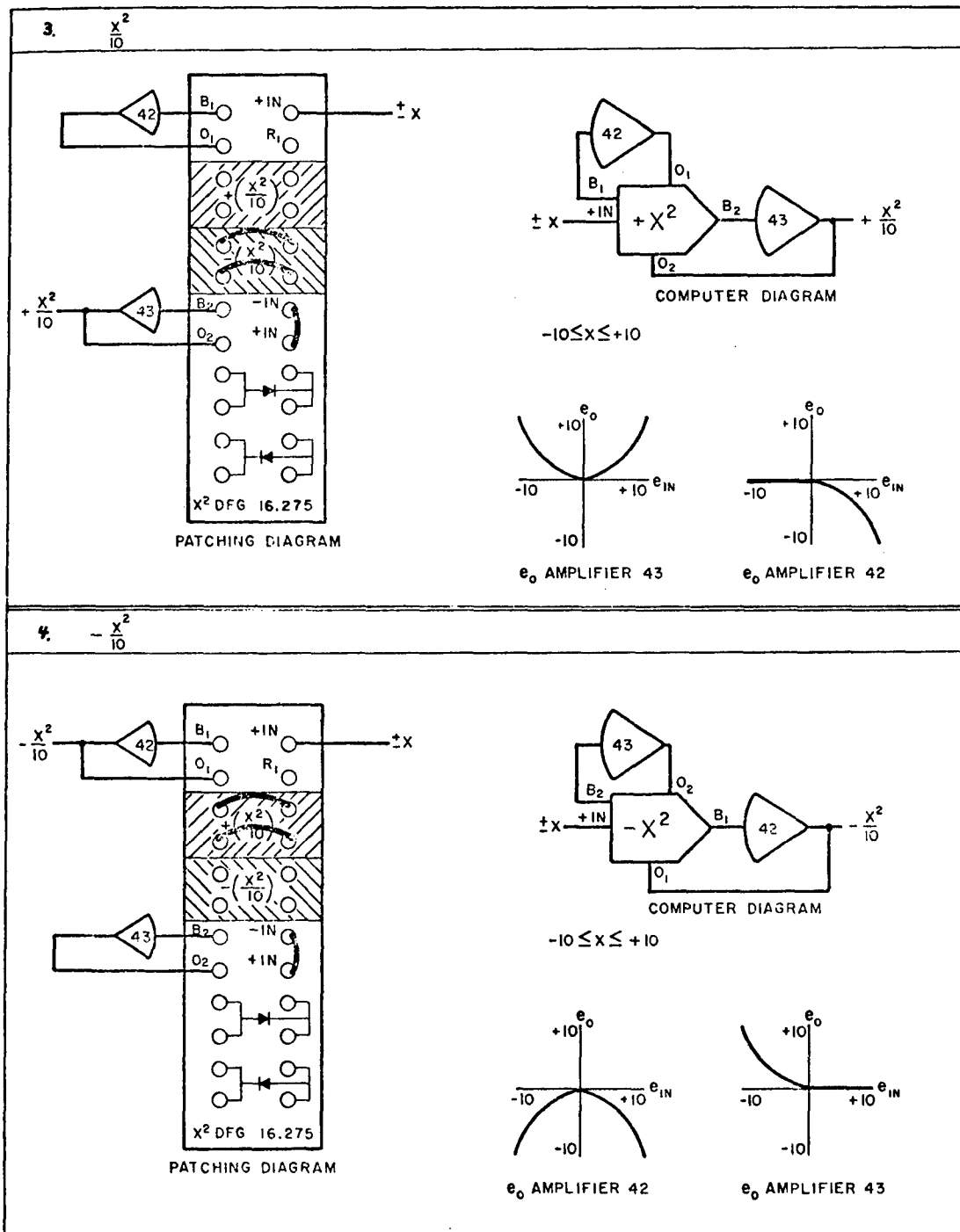
TABLE 2
COMMON NONLINEAR ANALOG COMPONENTS

QUARTER-SQUARE MULTIPLIER CIRCUITS



Courtesy of EAI-TR-48 Reference Guide

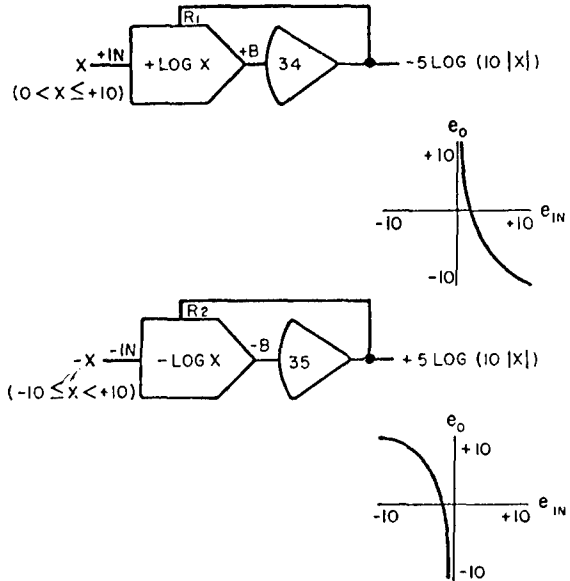
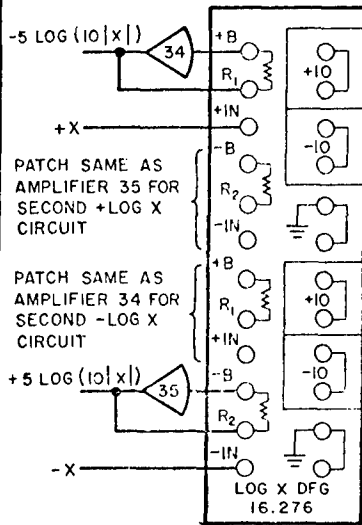
x^2 DFG CIRCUITS



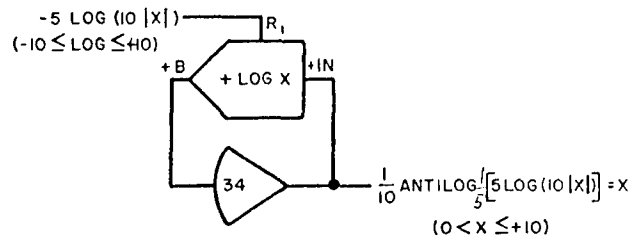
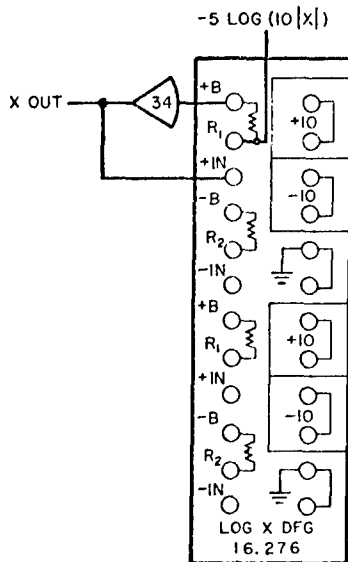
Courtesy of EAI-TR-48 Reference Guide

LOG X AND $\frac{1}{2}$ LOG X DFG CIRCUITS

5. $-\text{LOG}_{10} X$ FOR $+X$ INPUT AND $+\text{LOG}_{10} X$ FOR $-X$ INPUT

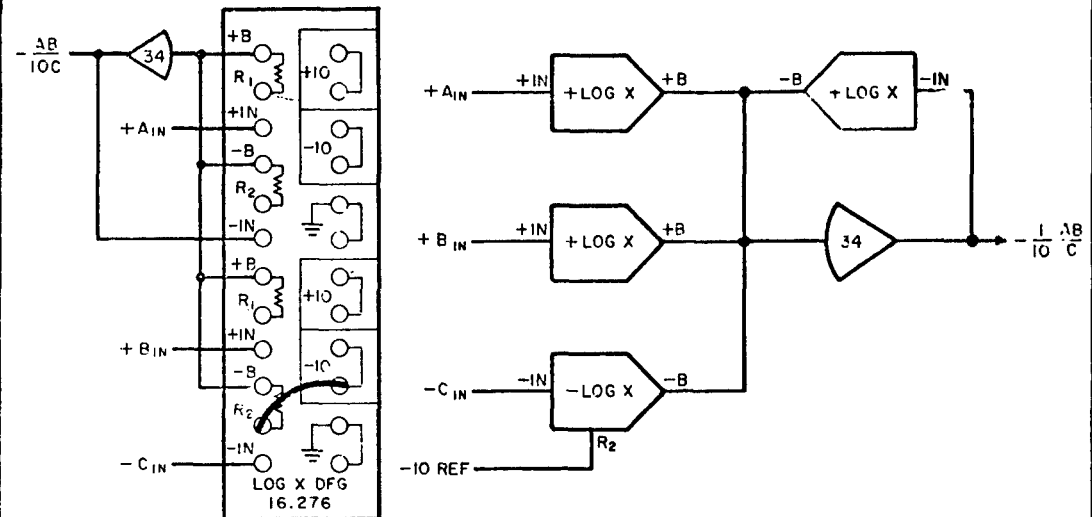


6. ANTILOG, BASE 10

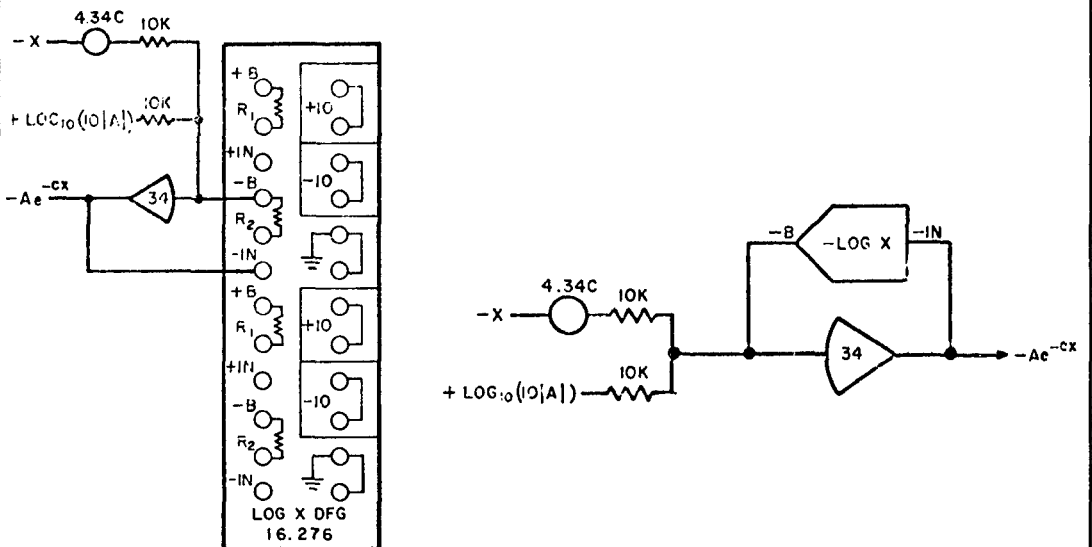


Courtesy of EAI-TR-48 Reference Guide

7. MULTIPLICATION AND DIVISION (MORE THAN TWO VARIABLES)



8. EXPONENTIAL



Courtesy of EAI-TR-48 Reference Guide

TABLE 3
WEIBULL SHAPE PARAMETER $\hat{\alpha}$ FOR
FINAL CRACK SIZE DISTRIBUTION

a_i (mils)	N = 8 Kc $v = 0.4$	10 Kc 0.5	13.3 Kc 0.667	20 Kc 1
30	1.61	1.76	1.99	2.16
40	1.36	1.49	1.63	1.71
50	1.28	1.33	1.49	1.70
60	1.12	1.20	1.33	---*
70	1.41	1.45	1.15	1.00

*Data for $a_i = 60$ mils, N = 20 Kc were lost.

TABLE 4
WEIBULL SCALE PARAMETER $\hat{\beta}$ (mils) FOR
FINAL CRACK SIZE DISTRIBUTION

a_i (mils)	N = 8 Kc $v = 0.4$	10 Kc 0.5	13.3 Kc 0.667	20 Kc 1
30	2.71	3.38	4.58	7.55
40	4.15	5.41	8.01	13.42
50	10.17	12.72	19.12	28.63
60	12.42	15.84	23.16	43.5*
70	18.72	23.51	37.43	71.35

*Estimated from empirical correlation

$$\beta = 2.34 \times 10^{-3} (va_i^2)^{1.2}$$

TABLE 5

RISK $R_f(a_{cr} | a_i, v)$ FOR $a_{cr} = 122$ MILS

a_i (mils)	Service Fraction v			
	0.4	0.5	2/3	1
20	1.00×10^{-391}	1.00×10^{-261}	3.98×10^{-157}	1.00×10^{-76}
30	3.16×10^{-80}	1.00×10^{-53}	7.08×10^{-33}	3.80×10^{-16}
40	1.26×10^{-24}	7.94×10^{-17}	1.82×10^{-10}	2.02×10^{-5}
50	1.26×10^{-9}	8.21×10^{-7}	2.63×10^{-4}	1.74×10^{-2}
60	1.74×10^{-4}	2.88×10^{-3}	2.89×10^{-2}	1.84×10^{-1}
70	2.14×10^{-2}	7.51×10^{-2}	2.14×10^{-1}	4.65×10^{-1}
80	1.74×10^{-1}	3.07×10^{-1}	4.91×10^{-1}	7.08×10^{-1}
90	4.64×10^{-1}	5.95×10^{-1}	7.33×10^{-1}	8.60×10^{-1}
100	7.31×10^{-1}	8.16×10^{-1}	8.85×10^{-1}	9.41×10^{-1}

TABLE 6
COMBINED RISK FOR a_i TO $a_{cr} = 122$ MILS

a_i (mils)	$f_i(a_i)\Delta a^*$	Products $R_f(a_{cr} a_i, v)f_i(a_i)\Delta a$ at Fraction v			
		0.4	0.5	2/3	1
20	.1602	1.60×10^{-392}	1.60×10^{-262}	6.38×10^{-158}	1.60×10^{-77}
30	.1010	3.19×10^{-81}	1.01×10^{-54}	7.15×10^{-34}	3.84×10^{-17}
40	.0593	7.47×10^{-26}	4.70×10^{-18}	1.08×10^{-11}	1.20×10^{-6}
50	.0321	4.04×10^{-11}	2.64×10^{-8}	8.44×10^{-6}	5.59×10^{-4}
60	.0192	3.34×10^{-6}	5.53×10^{-5}	5.55×10^{-4}	3.53×10^{-3}
70	.0128	2.74×10^{-4}	9.61×10^{-4}	2.74×10^{-3}	5.95×10^{-3}
80	.0112	1.95×10^{-3}	3.44×10^{-3}	5.50×10^{-3}	7.93×10^{-3}
90	.00961	4.45×10^{-3}	5.71×10^{-3}	7.04×10^{-3}	8.26×10^{-3}
100	.00801	5.85×10^{-3}	6.54×10^{-3}	7.09×10^{-3}	7.54×10^{-3}
Σ		1.25×10^{-2}	1.67×10^{-2}	2.29×10^{-2}	3.38×10^{-2}

* Computed from "Mechanized Probe" curve (Fig. 35).

TABLE 7

CRACK GROWTH BEHAVIOR UNDER CENTRAL LOADING

a_i (mils)	a_f (mils) at Service Fraction v			
	0.4	0.5	2/3	1
20	20.5	20.7	20.9	21.4
30	31.2	31.6	32.0	33.2
40	42.2	42.8	43.7	46.0
50	53.4	54.5	56.0	59.6
60	65.0	65.5	68.8	74.4
70	76.9	78.9	82.3	90.4
80	89.1	92.0	96.5	108.0
90	102.0	105.4	111.6	127.0
100	115.0	119.2	127.0	
110	128.0	133.5		

TABLE 8
HYPOTHETICAL DISTRIBUTIONS FOR
INITIAL FLAWS

a_i (mils)	$f_{mfg}(a_i) \Delta a$			$f_i(a_i) \Delta a$		
	CV=0.2	CV=0.3	CV=0.4	CV=0.2	CV=0.3	CV=0.4
10	---	.0114	.0540	---	.0314	.1063
20	.0044	.0540	.1295	.0140	.0985	.1685
30	.0540	.1828	.2420	.1110	.2140	.2020
40	.2420	.3256	.3521	.3200	.2475	.1912
50	.3989	.3989	.3989	.3600	.2075	.1440
60	.2420	.3256	.3521	.1640	.1265	.0977
70	.0540	.1828	.2420	.0291	.0568	.0538
80	.0044	.0540	.1295	.0020	.0140	.0239
90	1.36×10^{-5}	.0114	.0540	5.04×10^{-6}	.0024	.00824
100	1.49×10^{-7}	3.28×10^{-6}	.0175	4.50×10^{-8}	5.74×10^{-7}	.00217
110	---	---	.0044	---	---	.00044
120	---	---	4.38×10^{-5}	---	---	3.60×10^{-6}

TABLE 9
COMBINED RISK FOR a_i TO a_{cr} (CV=0.2)

a_i (mils)	$f_i(a_i)\Delta a$ (Table 12)	Products $R_f(a_{cr} a_i, v)f_i(a_i)\Delta a$ at Fraction v			
		0.4	0.5	2/3	1
40	.3200	4.03×10^{-25}	2.54×10^{-17}	5.82×10^{-11}	6.46×10^{-6}
50	.3600	4.54×10^{-10}	2.95×10^{-7}	9.47×10^{-5}	6.26×10^{-3}
60	.1640	2.86×10^{-5}	4.72×10^{-4}	4.74×10^{-3}	3.02×10^{-2}
70	.0291	6.24×10^{-4}	2.18×10^{-3}	6.24×10^{-3}	1.35×10^{-2}
80	.0020	3.48×10^{-4}	6.14×10^{-4}	9.82×10^{-4}	1.42×10^{-3}
90	5.04×10^{-6}	2.34×10^{-6}	3.00×10^{-6}	3.69×10^{-6}	4.34×10^{-6}
100	4.50×10^{-8}	3.29×10^{-8}	3.68×10^{-8}	3.98×10^{-8}	4.24×10^{-8}
Σ		1.00×10^{-3}	3.27×10^{-3}	1.21×10^{-2}	5.14×10^{-2}

TABLE 10
COMBINED RISK FOR a_i TO a_{cr} (CV=0.3)

		Products $R_f(a_{cr} a_i, v) f_i(a_i) \Delta a$ at Fraction v			
a_i (mils)	$f_i(a_i) \Delta a$ (Table 12)				
40	.2475	3.12×10^{-25}	1.96×10^{-17}	4.50×10^{-11}	5.00×10^{-6}
50	.2075	2.62×10^{-10}	1.71×10^{-7}	5.46×10^{-5}	3.61×10^{-3}
60	.1265	2.20×10^{-5}	3.64×10^{-4}	3.66×10^{-3}	2.33×10^{-2}
70	.0568	1.21×10^{-3}	4.26×10^{-3}	1.21×10^{-2}	2.64×10^{-2}
80	.0140	2.44×10^{-3}	4.30×10^{-3}	6.86×10^{-3}	9.90×10^{-3}
90	.0024	1.11×10^{-3}	1.43×10^{-3}	1.76×10^{-3}	2.06×10^{-3}
100	5.74×10^{-7}	4.20×10^{-7}	4.63×10^{-7}	5.08×10^{-7}	5.41×10^{-7}
Σ		4.78×10^{-3}	1.04×10^{-2}	2.44×10^{-2}	6.53×10^{-2}

TABLE 11
COMBINED RISK FOR a_i TO a_{cr} (CV=0.4)

a_i (mils)	$f_i(a_i)\Delta a$ (Table 12)	Products $R_f(a_{cr} a_i, v)f_i(a_i)\Delta a$ at Fraction v			
		0.4	0.5	2/3	1
50	.1440	1.81×10^{-10}	1.18×10^{-7}	3.79×10^{-5}	2.51×10^{-3}
60	.0977	1.70×10^{-5}	2.81×10^{-4}	2.82×10^{-3}	1.80×10^{-2}
70	.0538	1.15×10^{-3}	4.04×10^{-3}	1.15×10^{-2}	2.50×10^{-2}
80	.0239	4.16×10^{-3}	7.35×10^{-3}	1.17×10^{-2}	1.69×10^{-2}
90	.00824	3.82×10^{-3}	4.90×10^{-3}	6.04×10^{-3}	7.09×10^{-3}
100	.00217	1.59×10^{-3}	1.77×10^{-3}	1.92×10^{-3}	2.04×10^{-3}
110	.00044	4.40×10^{-4}	4.40×10^{-4}	4.40×10^{-4}	4.40×10^{-4}
Σ		1.12×10^{-2}	1.88×10^{-2}	3.45×10^{-2}	7.20×10^{-2}

TABLE 12
COMPARISON OF RISKS TO 122 MILS

Risk Basis	Service Fraction ν			
	0.4	0.5	2/3	1
$\Sigma R_f i \Delta a$ + proof test to 0.1	.0125	.0167	.0229	.0338
$\Sigma R_f i \Delta a$ without proof test	.0553	.0595	.0657	.0766
Central behavior + proof test to 0.1	0	0	.0032	.0126
Central behavior without proof test	.0381	.0411	.0460	.0554
$\Sigma R_f i \Delta a$ (f_{mfg} with $CV=0.2$)	.0010	.0033	.0121	.0514
$\Sigma R_f i \Delta a$ (f_{mfg} with $CV=0.3$)	.0048	.0104	.0244	.0653
$\Sigma R_f i \Delta a$ (f_{mfg} with $CV=0.4$)	.0112	.0188	.0345	.0720

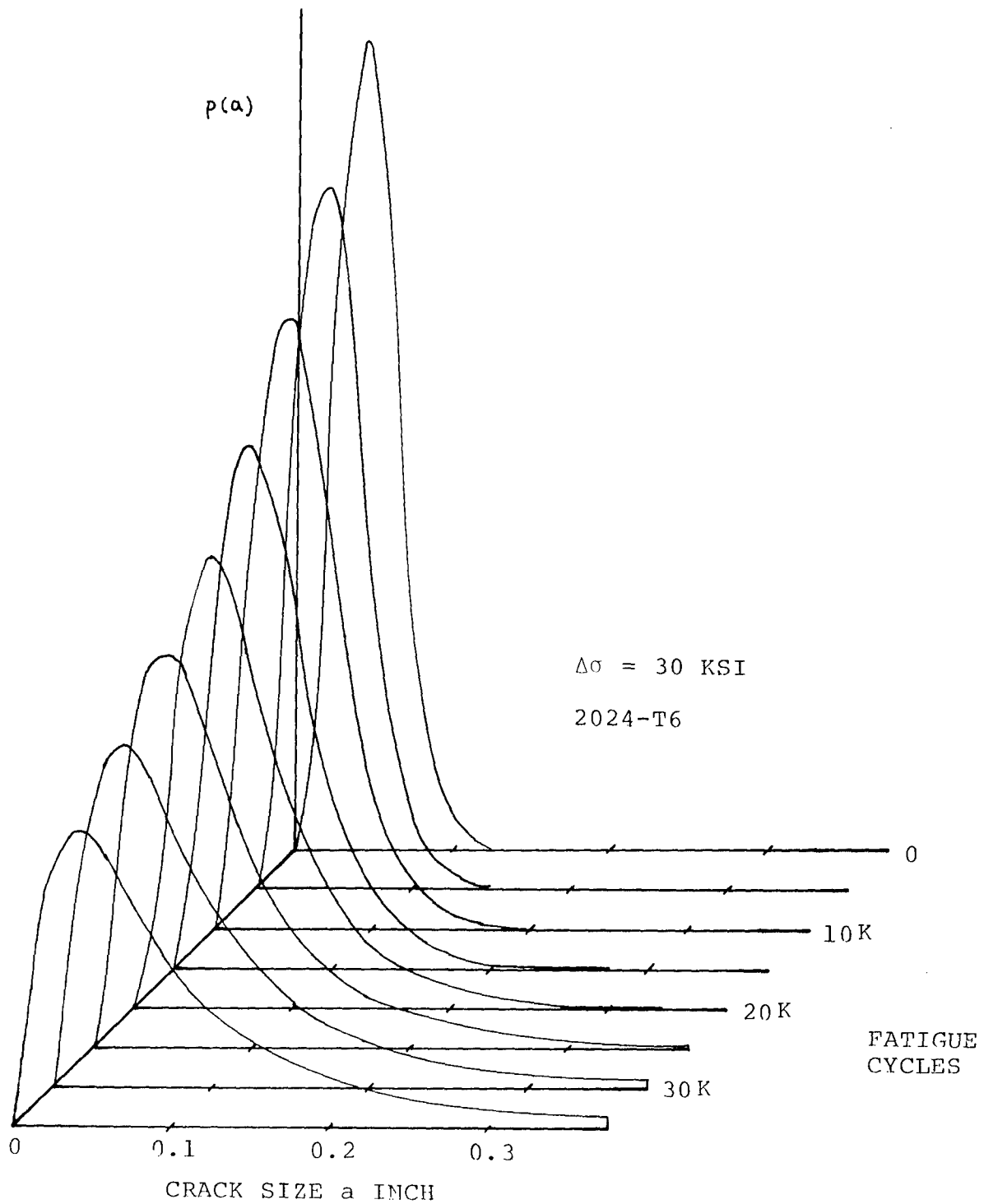
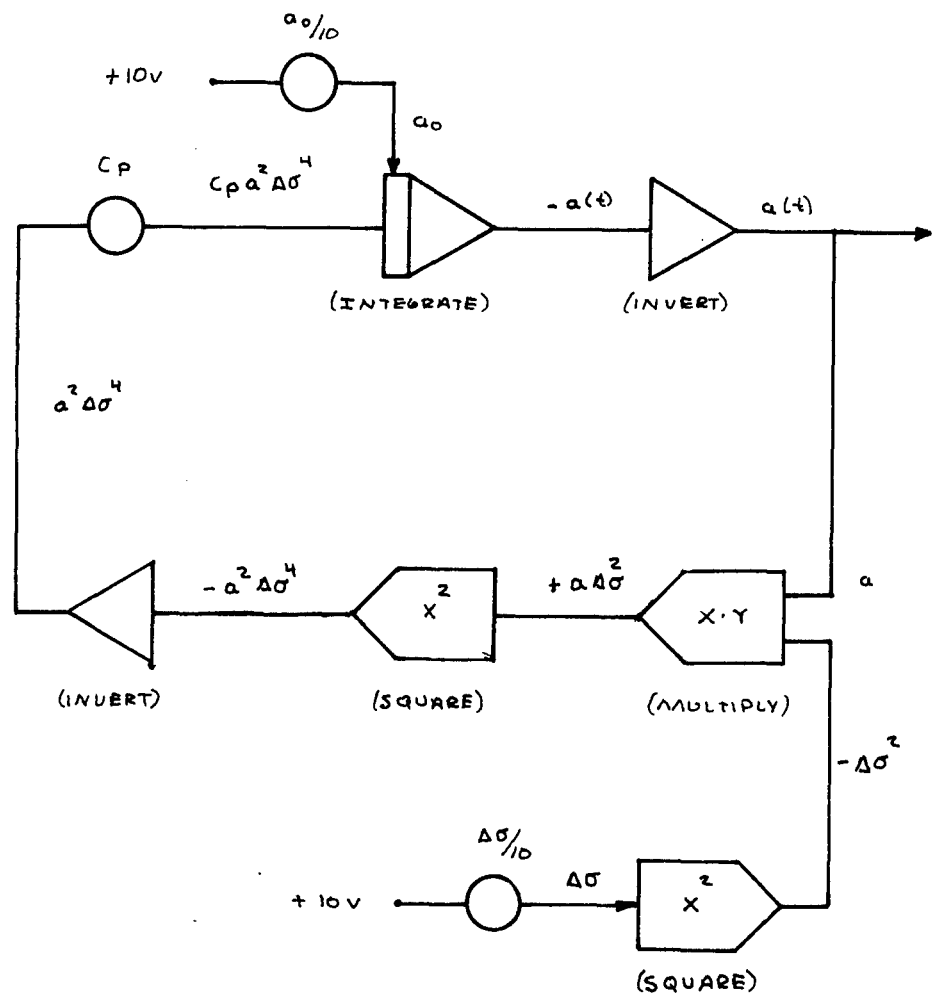


Figure 1: Weibull Distribution for Crack Size as a Function of Constant-Amplitude Fatigue



$$\frac{da}{dN} = C_p a^2 \Delta \sigma^4$$

$$N = t$$

$$N_p = 4$$

Figure 2: Paris Equation Analog Program Diagram

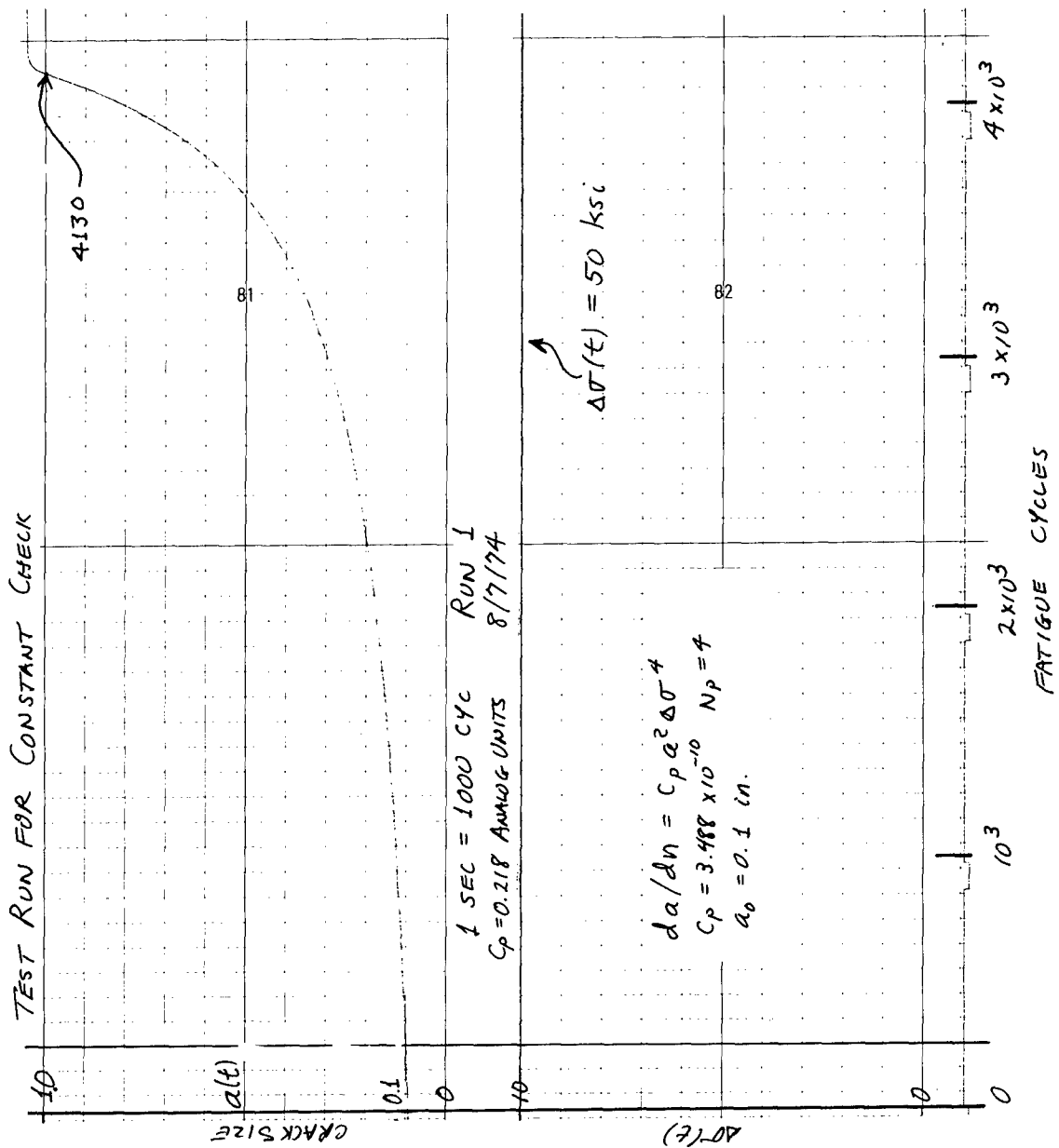
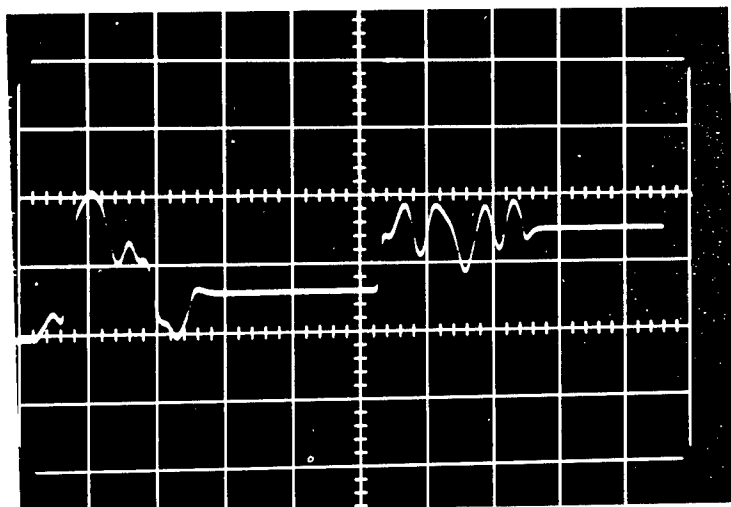


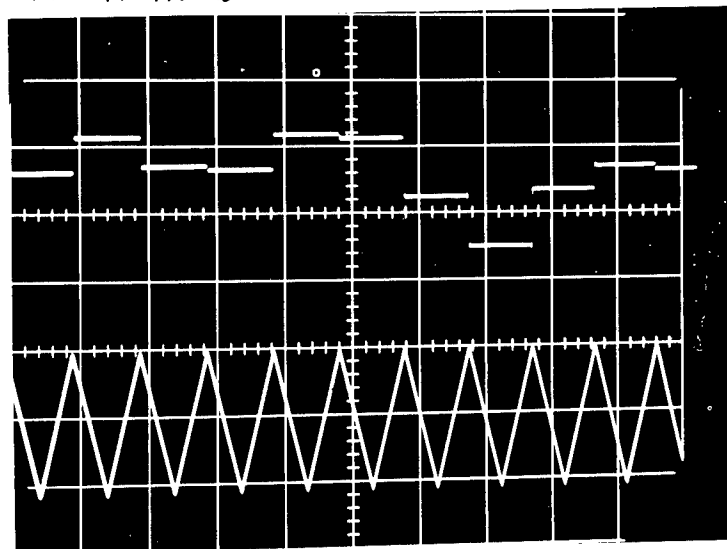
Figure 3: Typical Analog Crack Growth Solution for Constant-Amplitude Fatigue

TRACK-HOLD $1\text{ cm} \approx 0.2\text{ ms}$ 1000 Hz



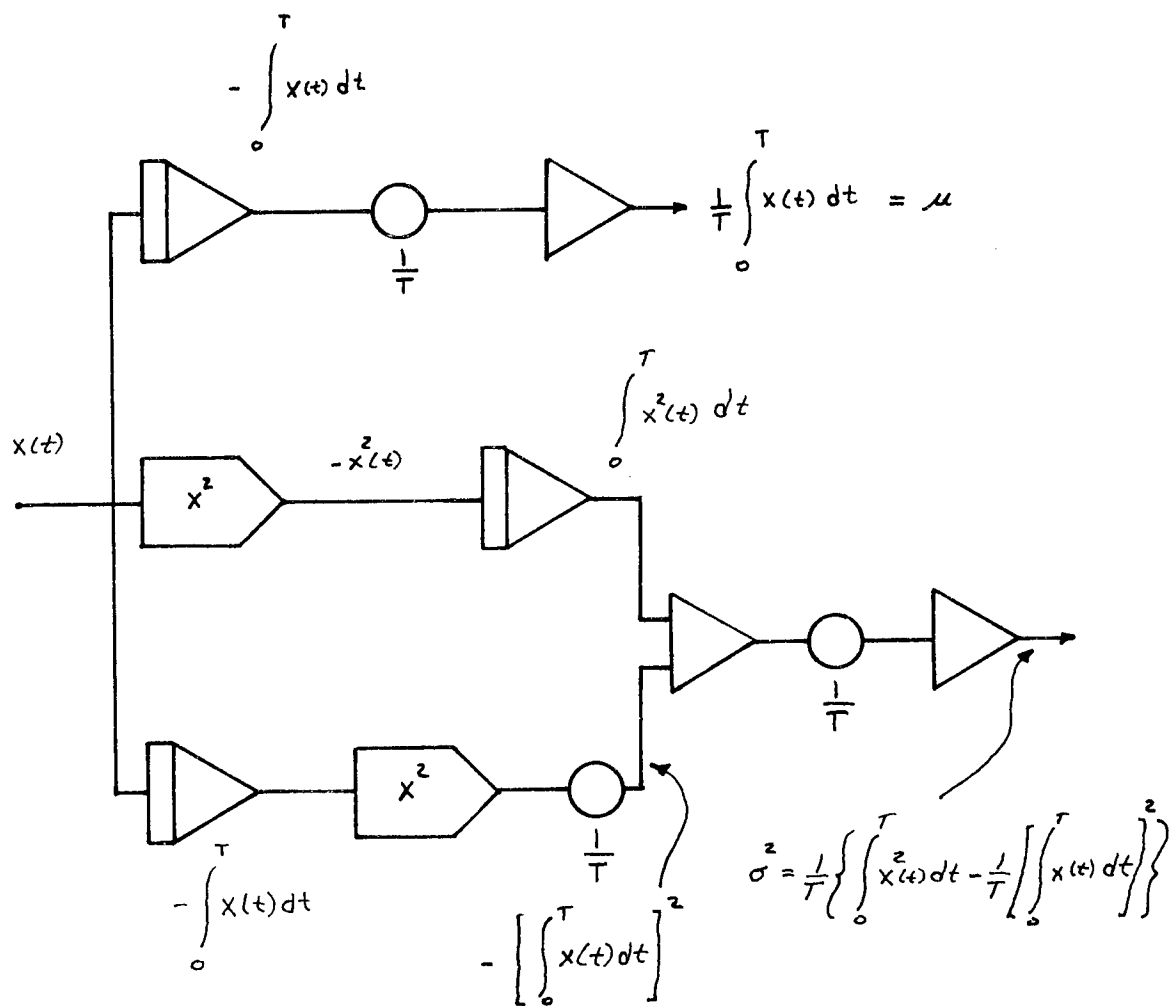
HALF TRACK - HALF HOLD

TRACK-HOLD $1\text{ cm} = 10\text{ ms}$ 100 Hz



MAX HOLD

Figure 5: Samples of Track-Hold Noise



μ and σ recorded at $t=T$

Figure 6: Analog Program Diagram for Mean and Standard Deviation

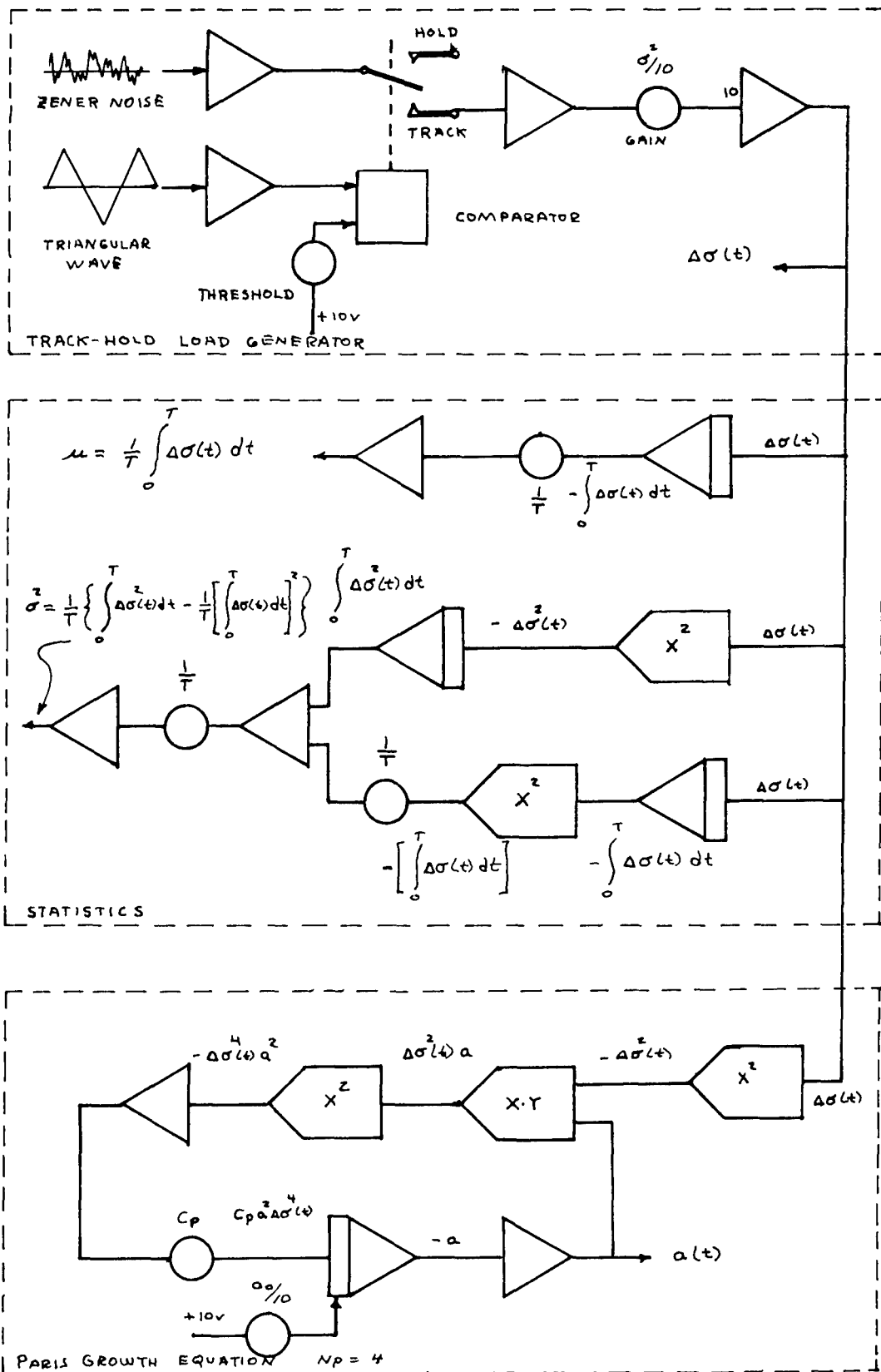


Figure 7: Analog Program Diagram for Paris Equation with Random Loading

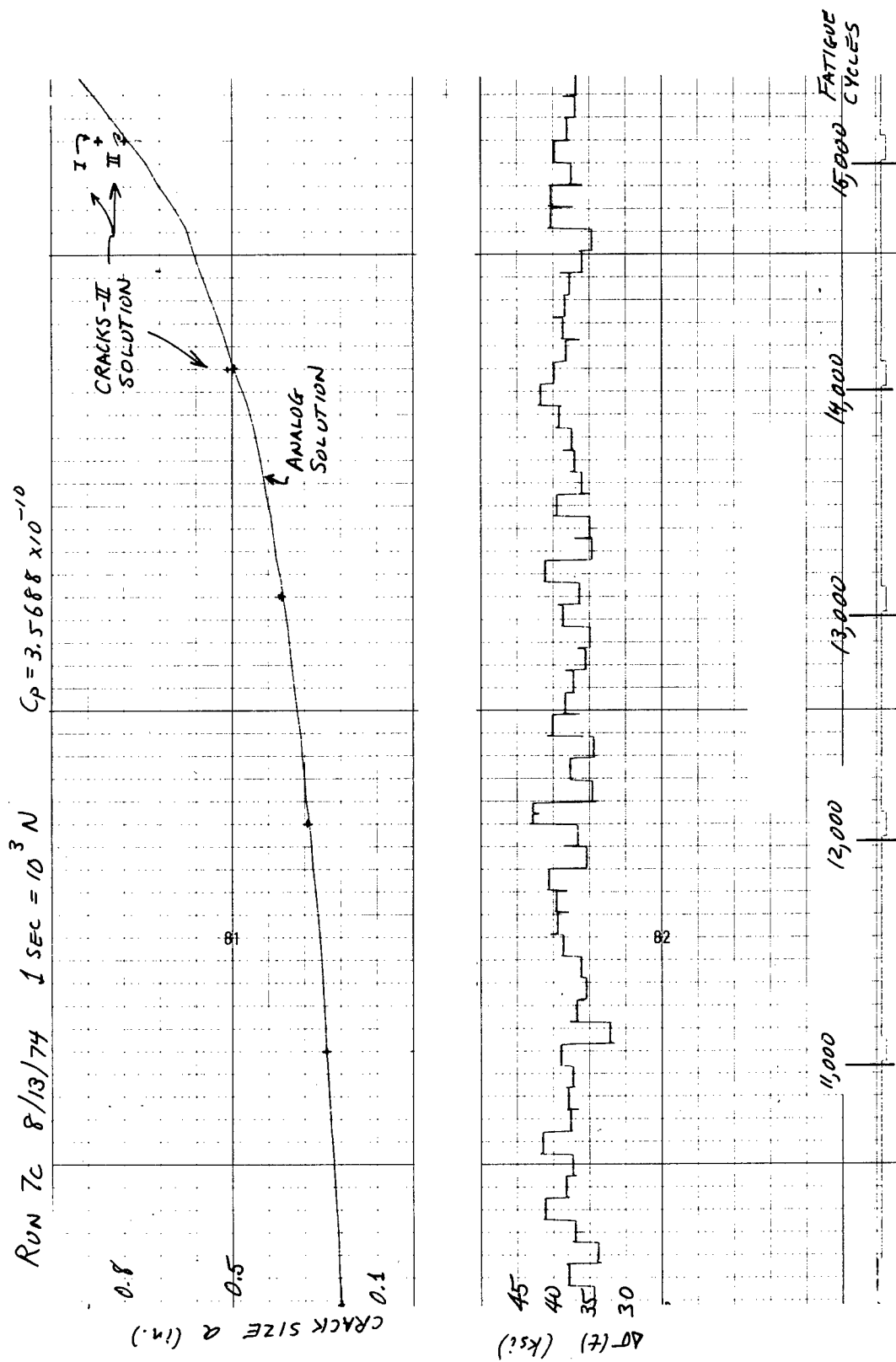


Figure 8: Typical Analog Crack Growth Solution for Random-Load Fatigue

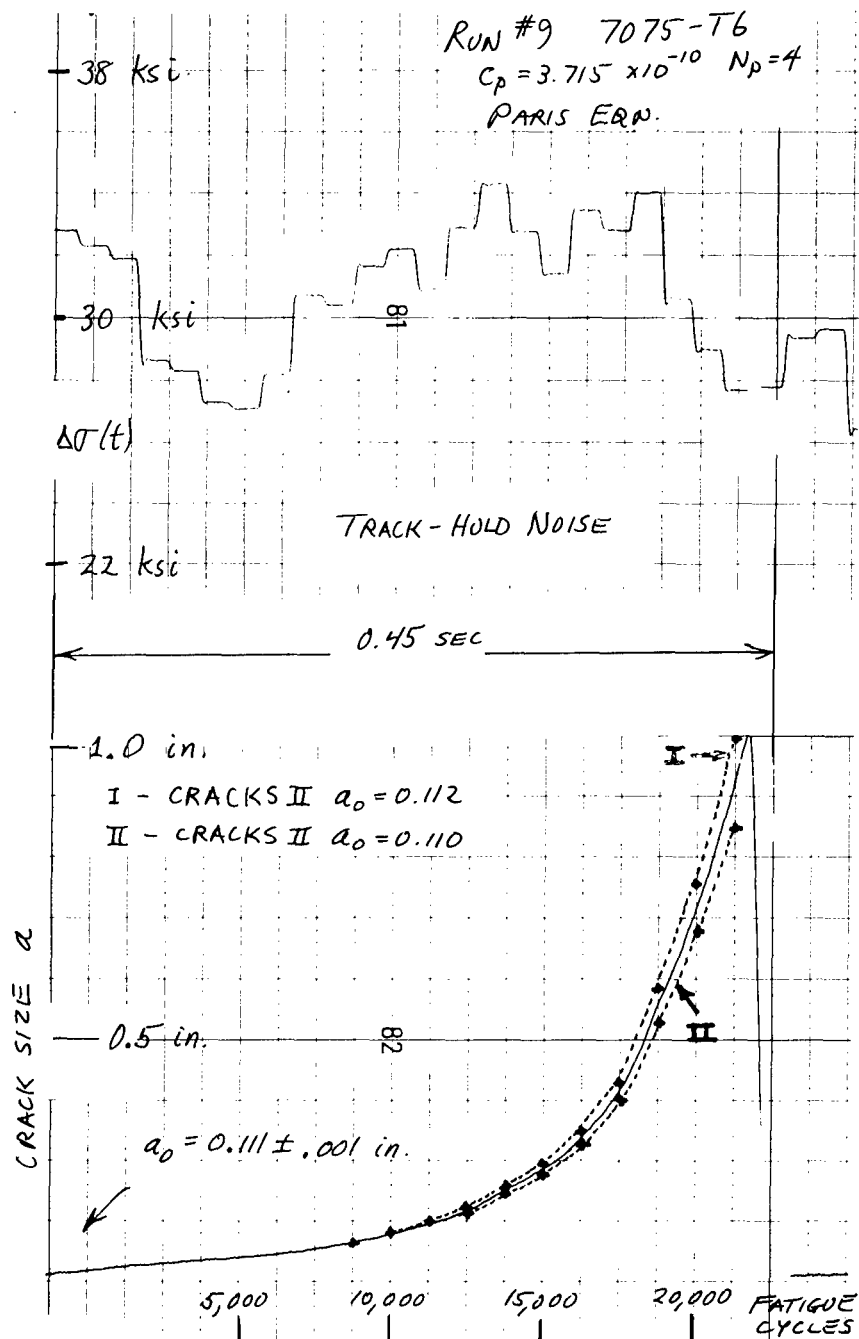


Figure 9: Typical Analog Random-Load Solution Using REPOP

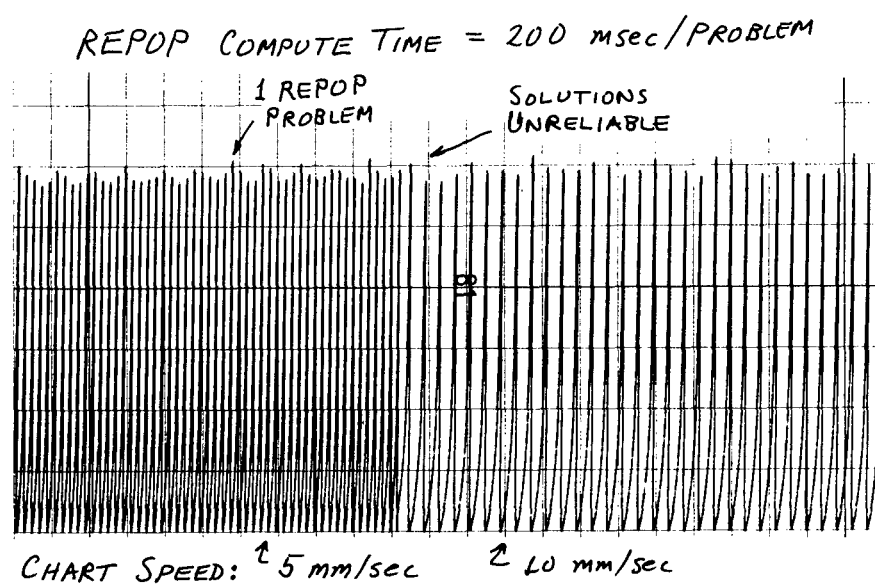


Figure 10: REPOP Switch Error

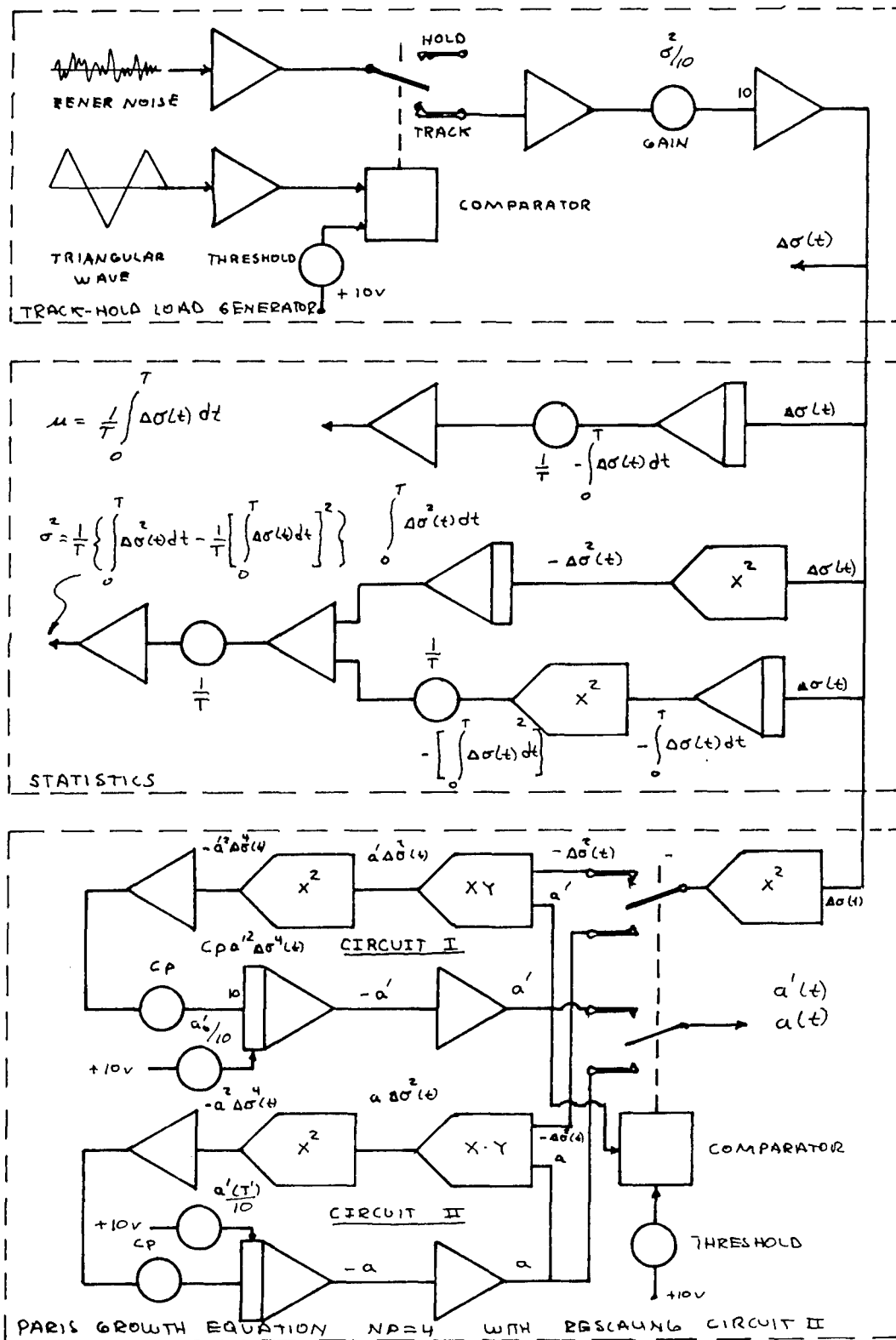


Figure 11: Analog Program Diagram for Paris Equation with Random Loading and Rescaling

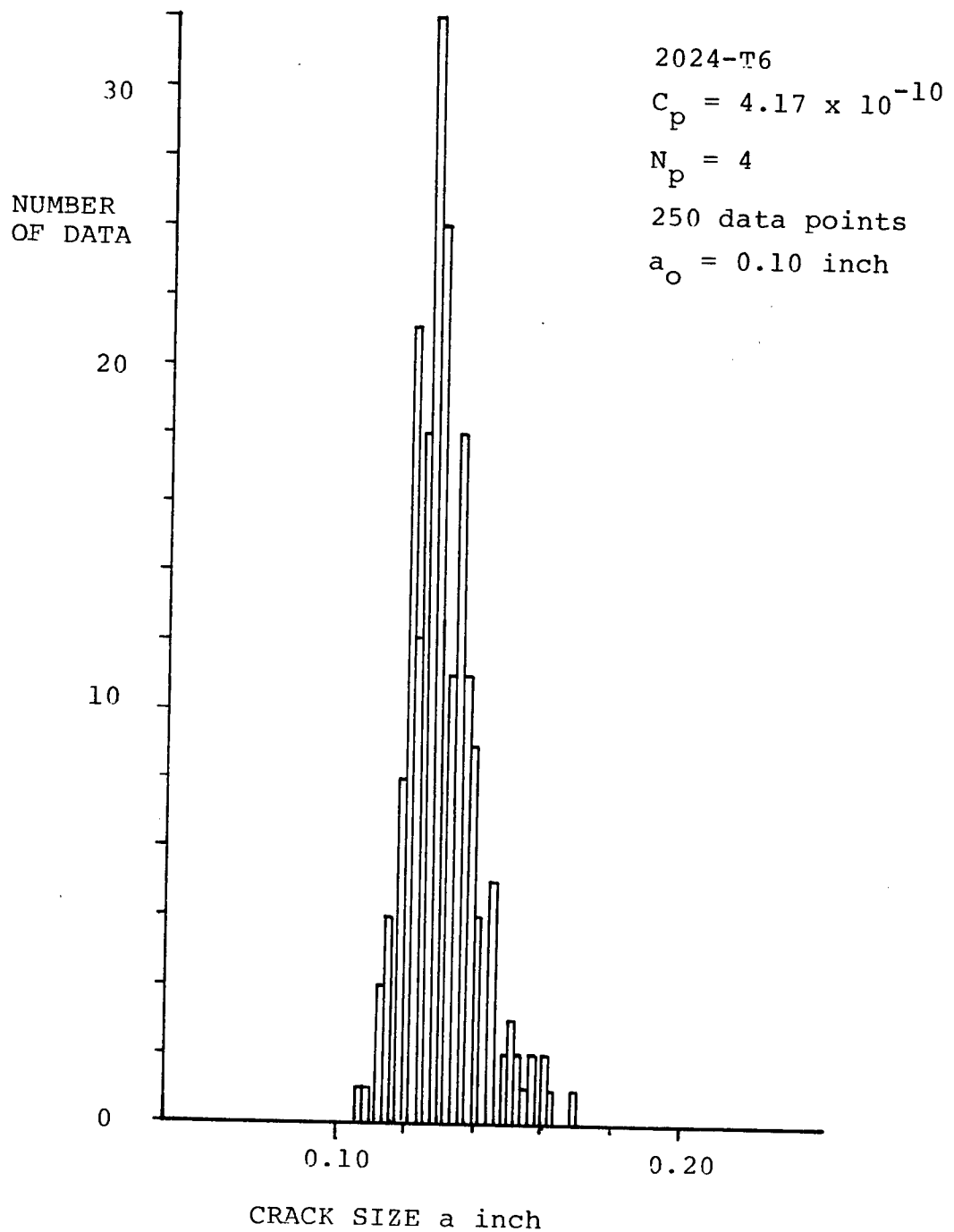


Figure 12: Histogram of Crack Size after 10,000 Fatigue Cycles

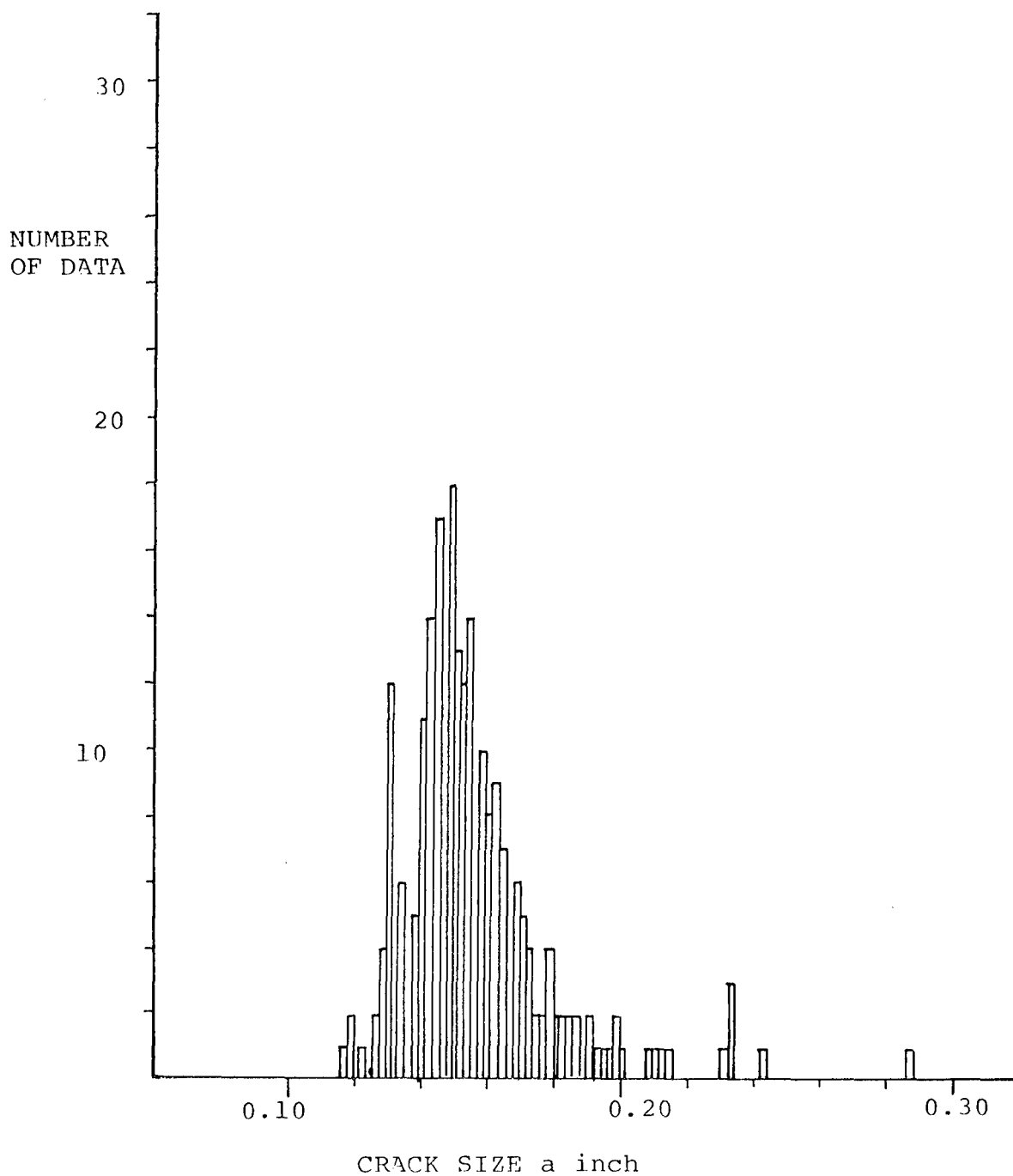


Figure 13: Histogram of Crack Size after 15,000 Fatigue Cycles

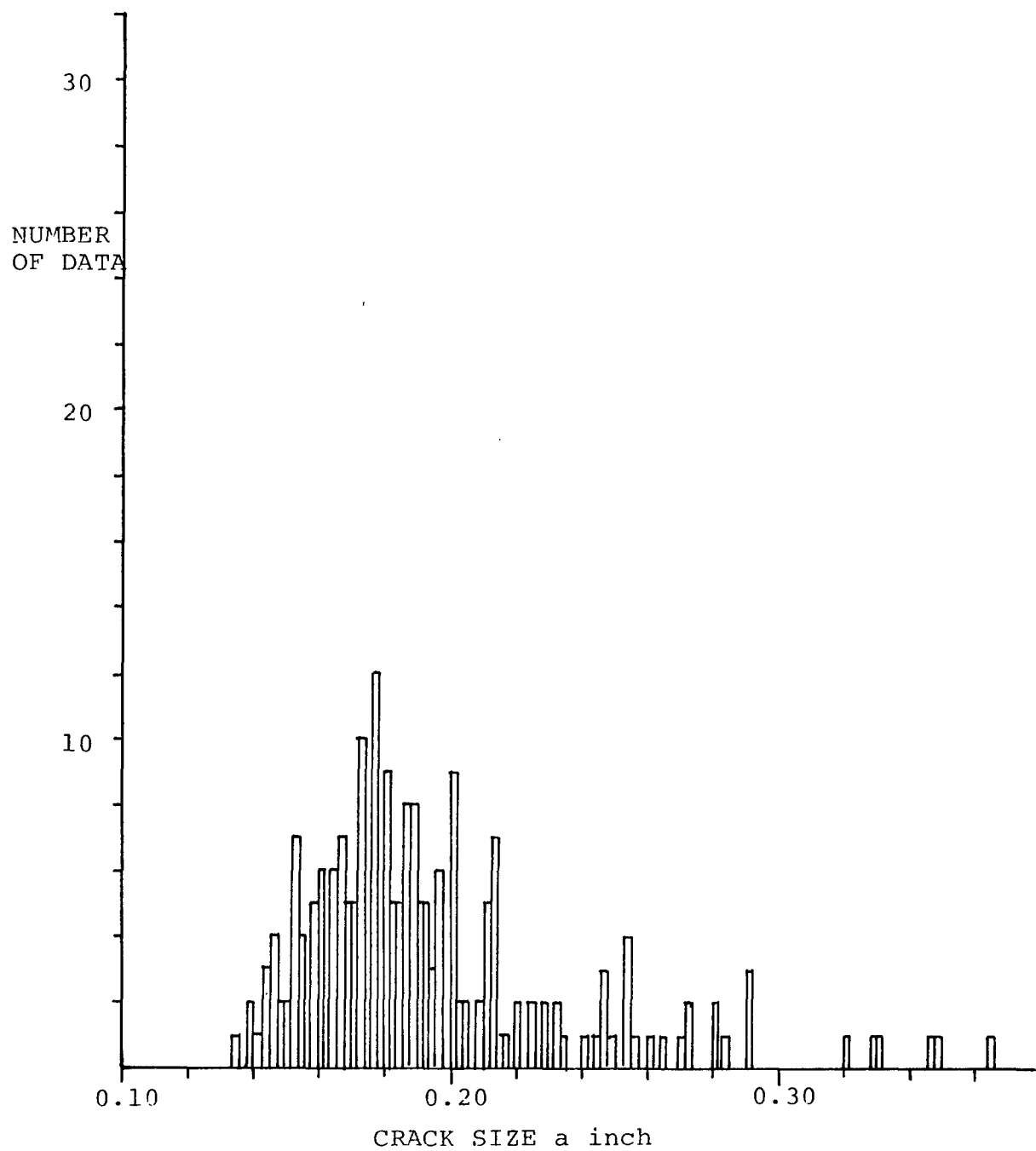


Figure 14: Histogram of Crack Size after 20,000 Fatigue Cycles

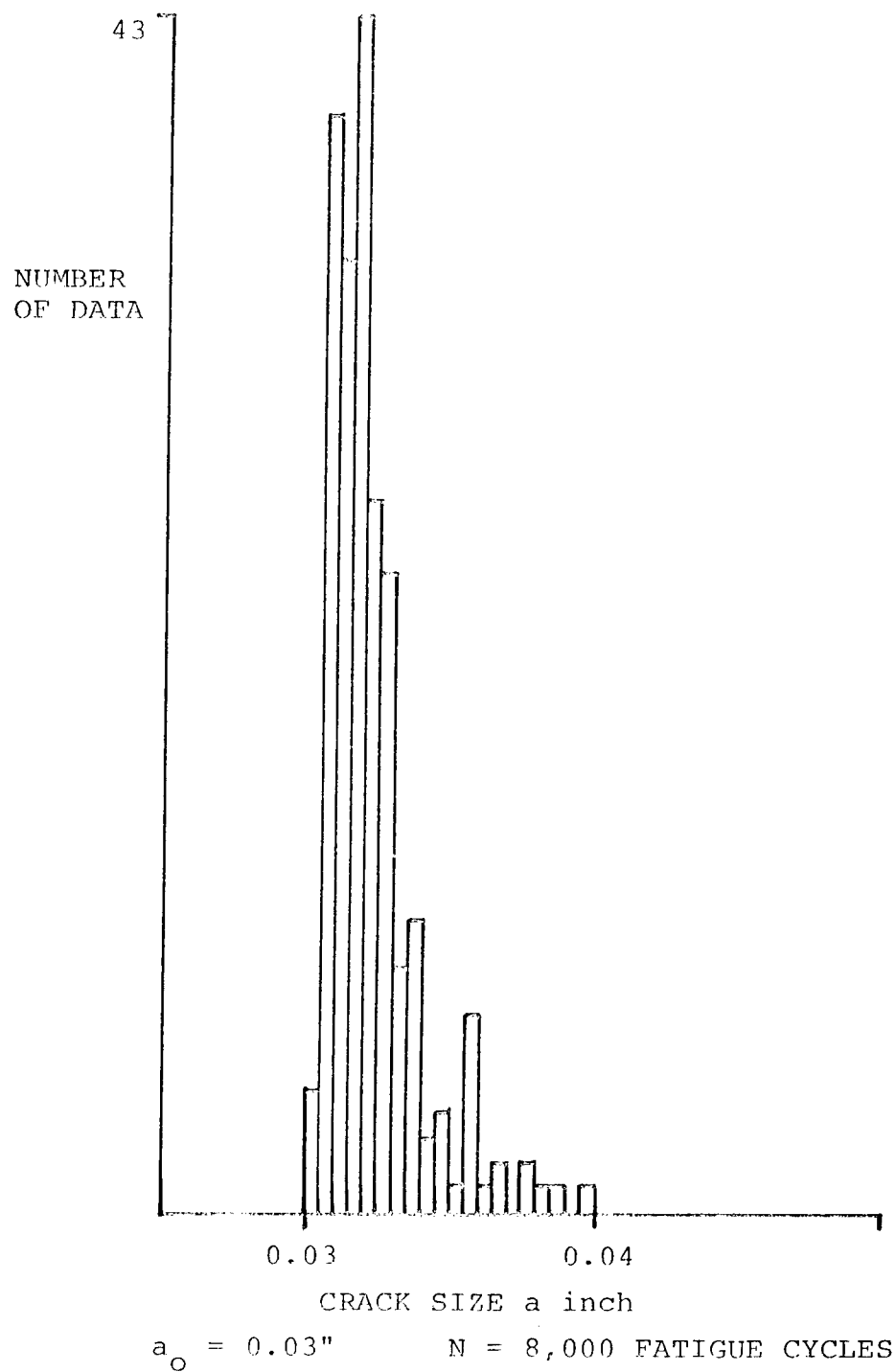


Figure 15: Crack Size Histogram ($a_i = .03$, $N = 8,000$)

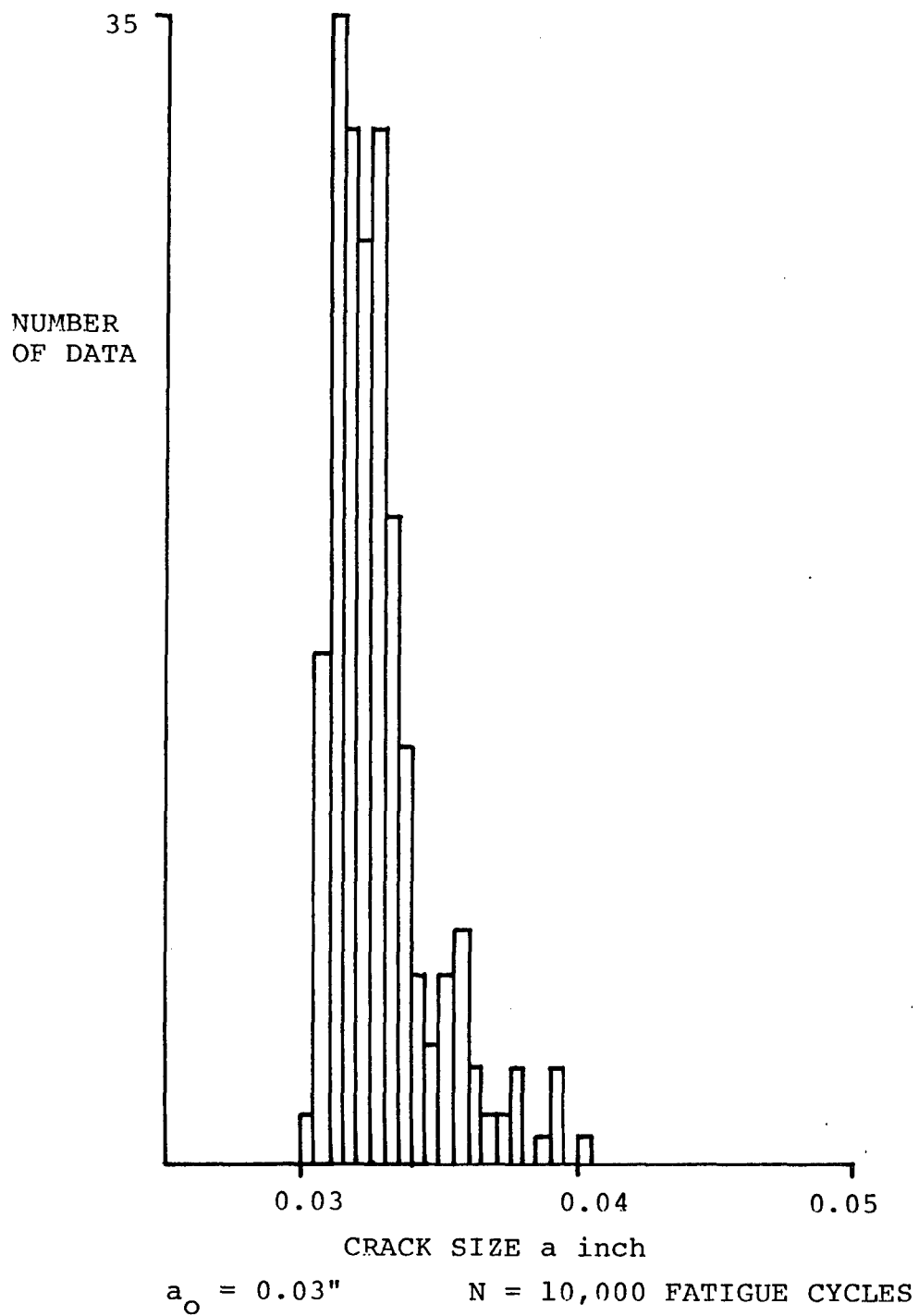


Figure 16: Crack Size Histogram ($a_i = .03$, $N = 10,000$)

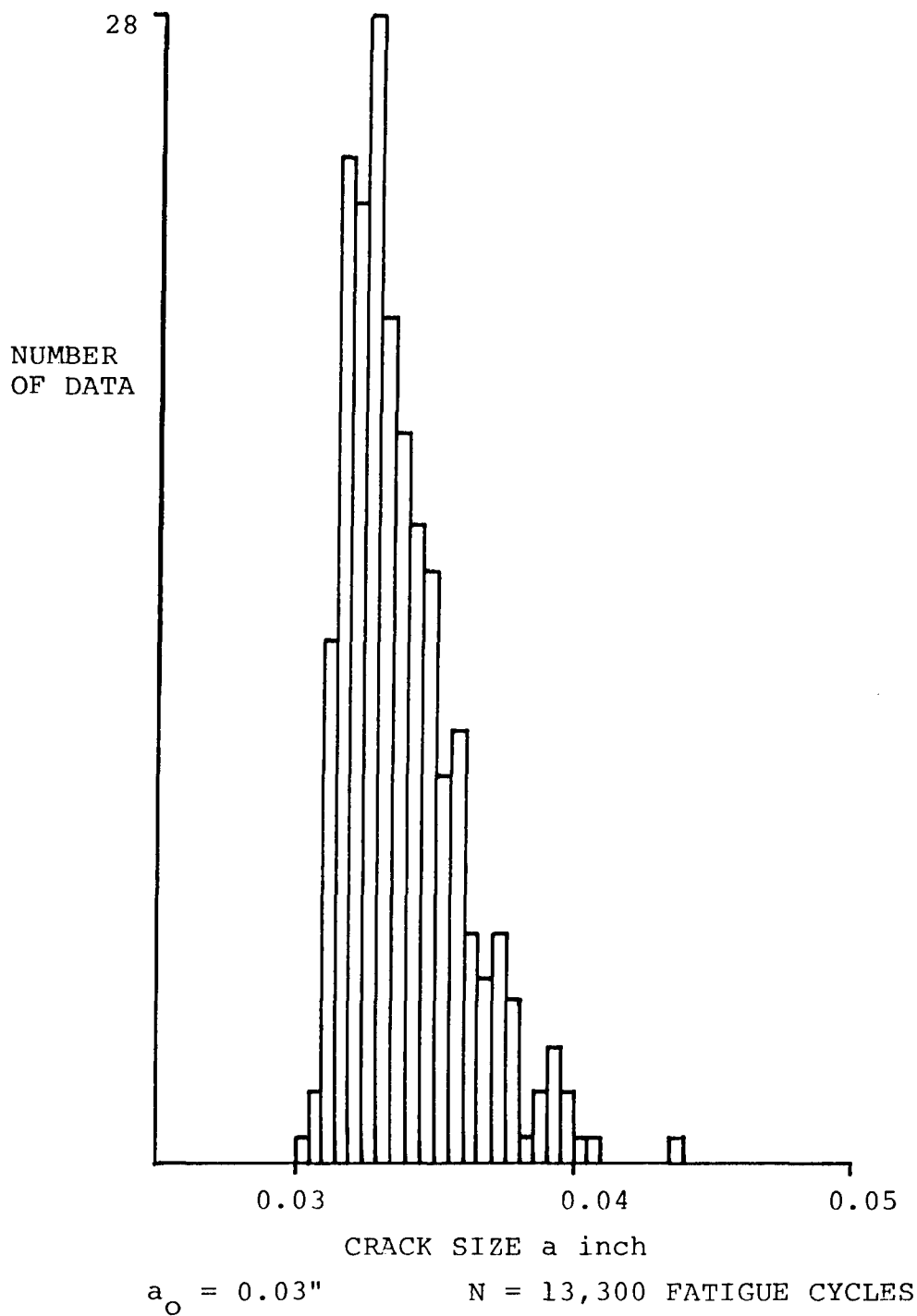


Figure 17: Crack Size Histogram ($a_i = .03$, $N = 13,300$)

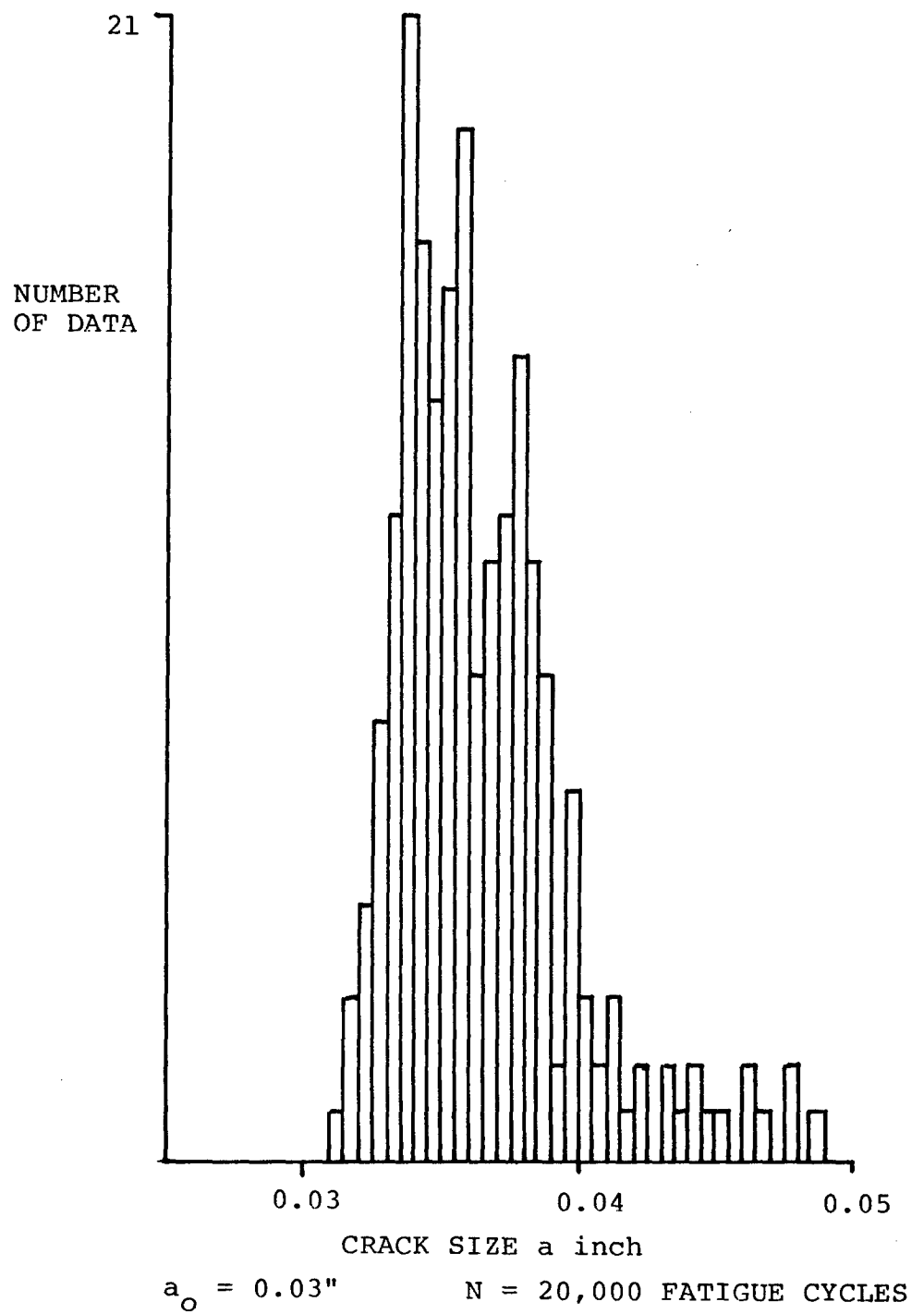


Figure 18: Crack Size Histogram ($a_i = .03$, $N = 20,000$)

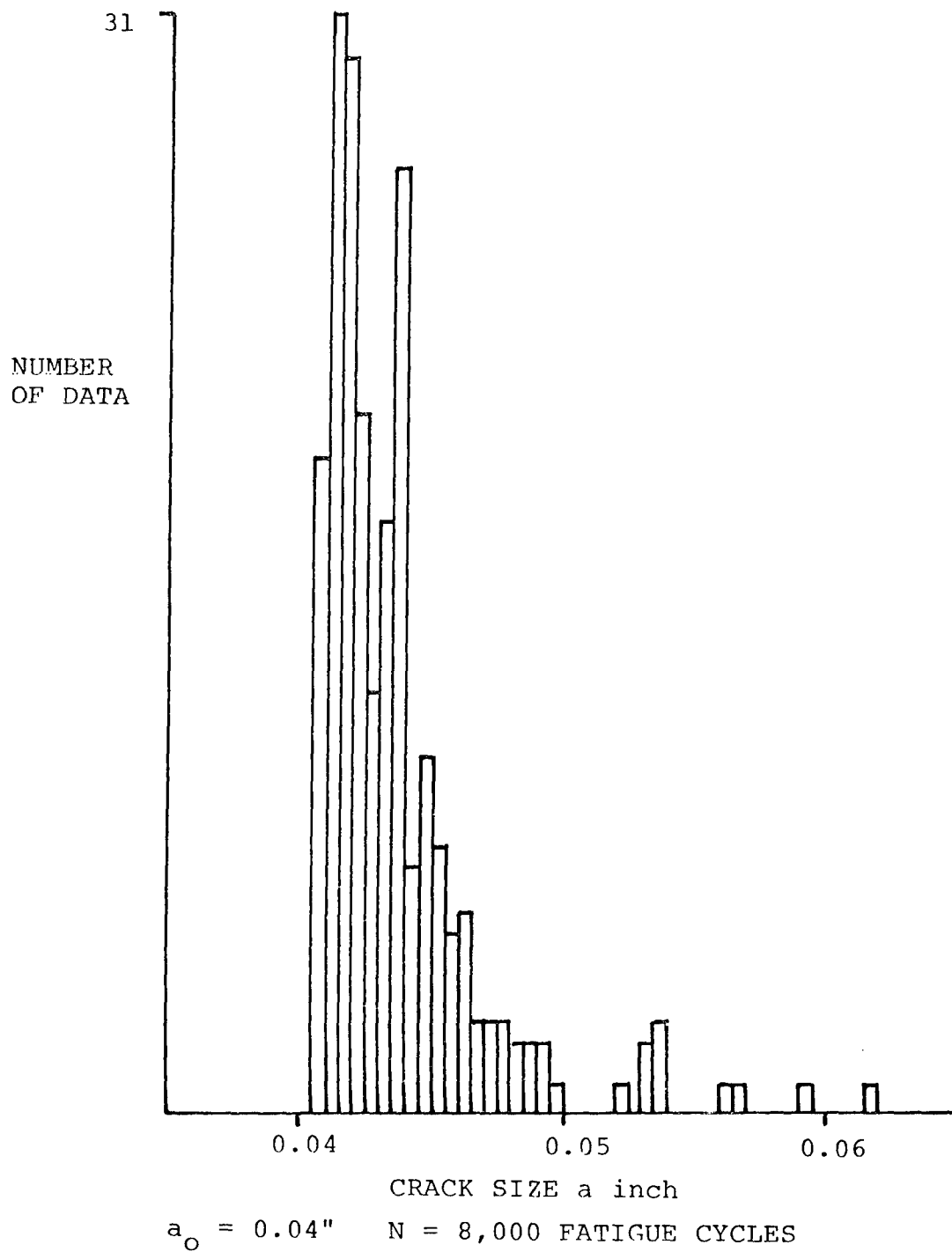


Figure 19: Crack Size Histogram ($a_i = .04$, $N = 8,000$)

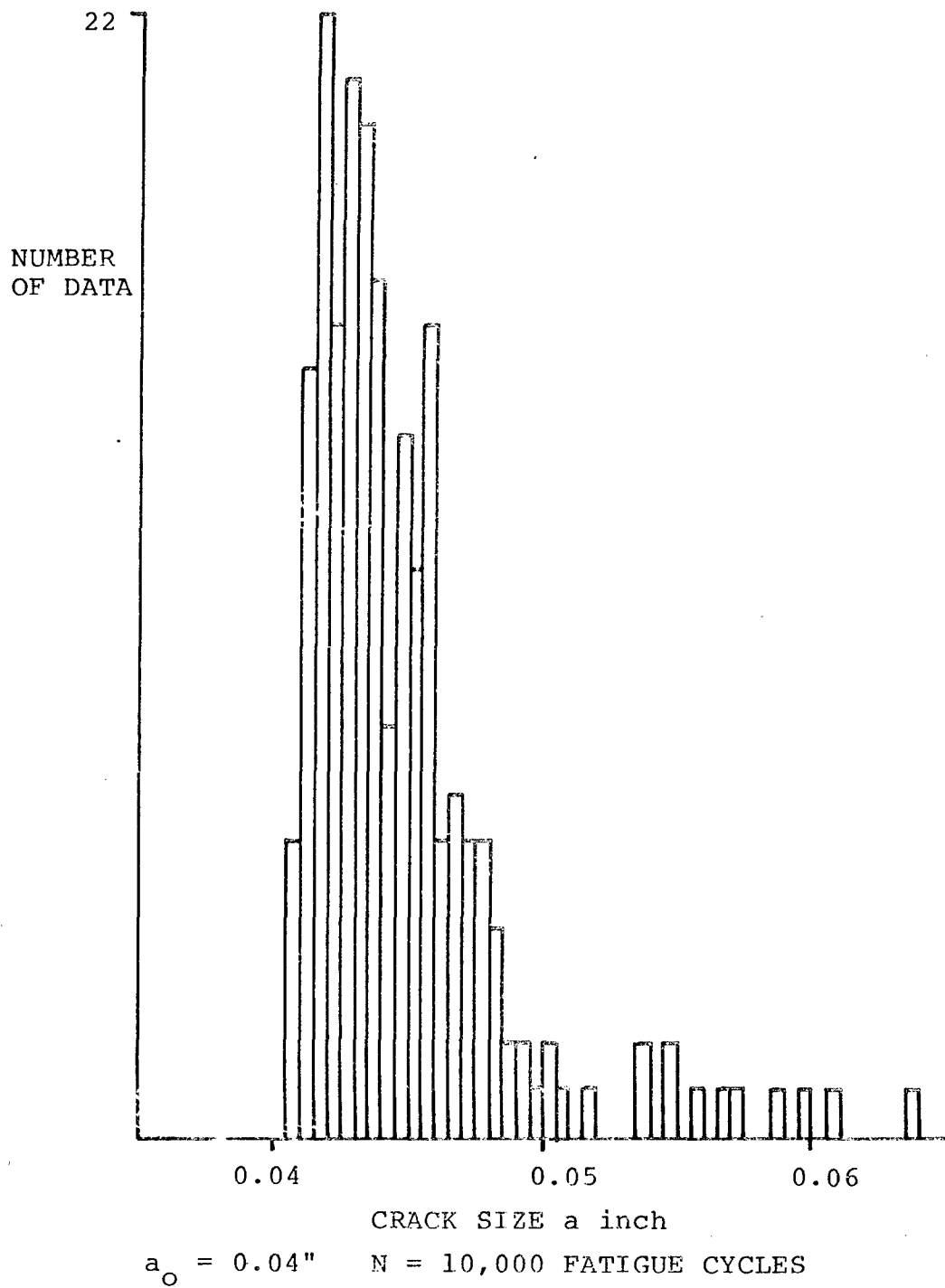


Figure 20: Crack Size Histogram ($a_i = .04$, $N = 10,000$)

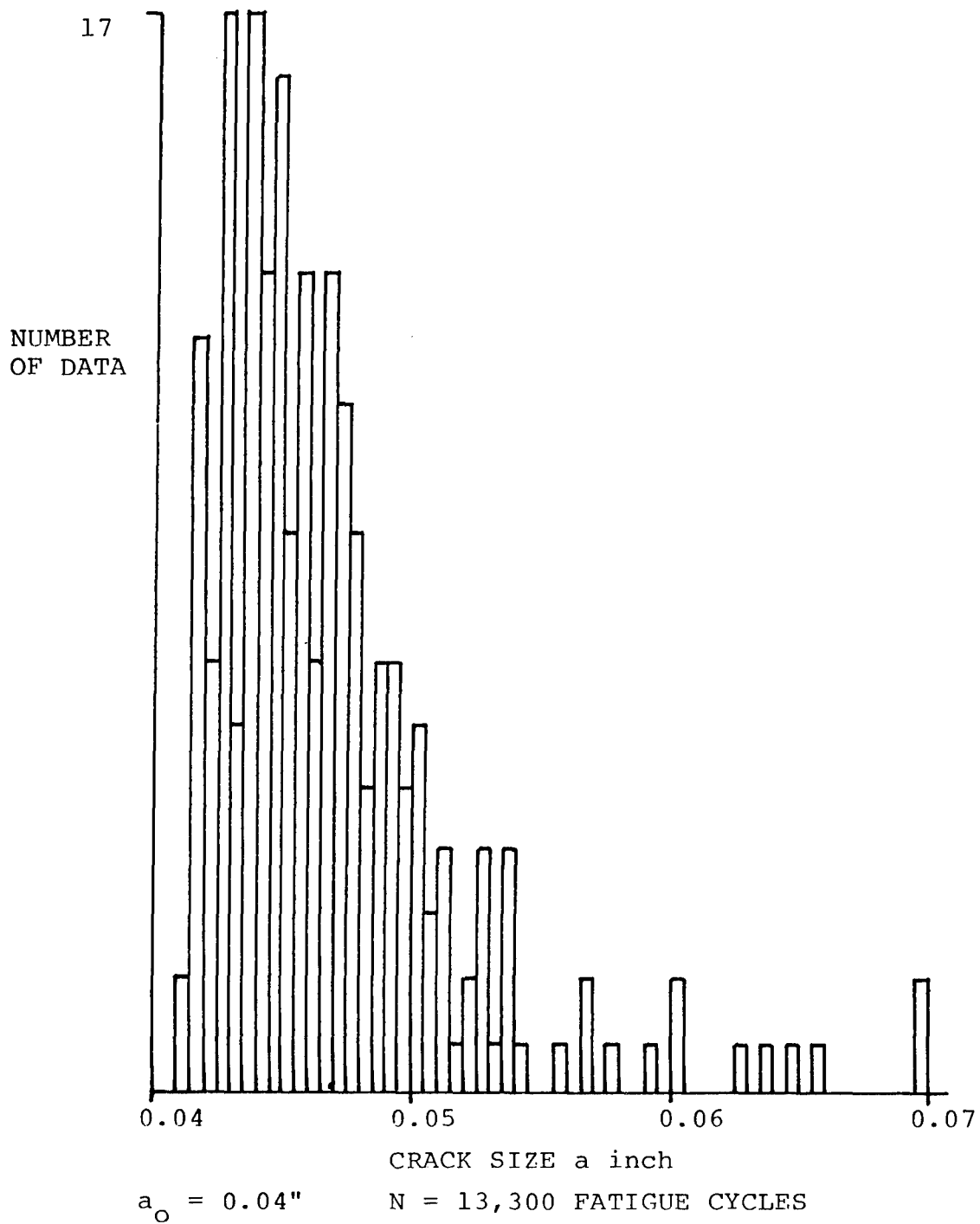


Figure 21: Crack Size Histogram ($a_i = .04$, $N = 13,300$)

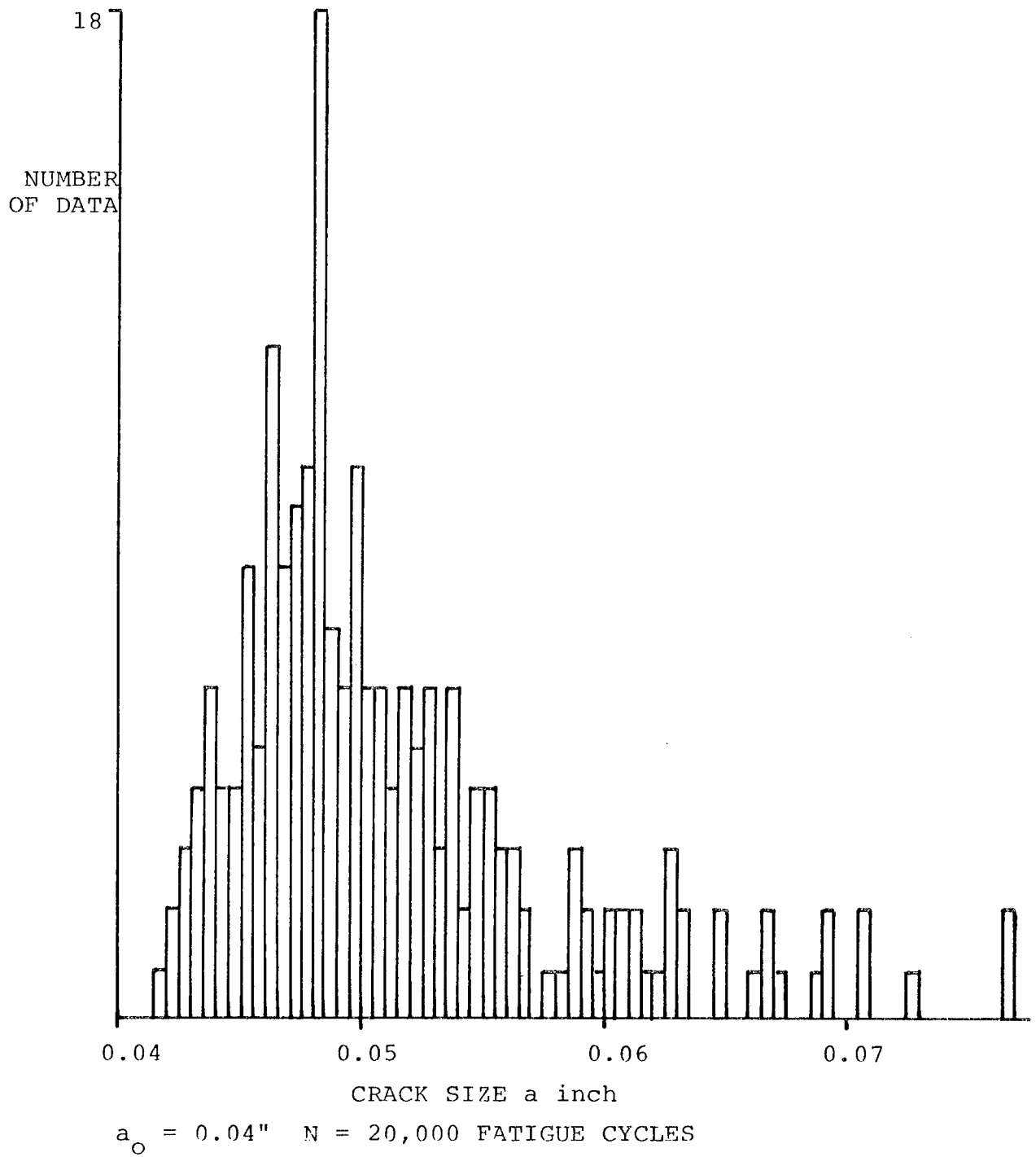


Figure 22: Crack Size Histogram ($a_i = .04$, $N = 20,000$)

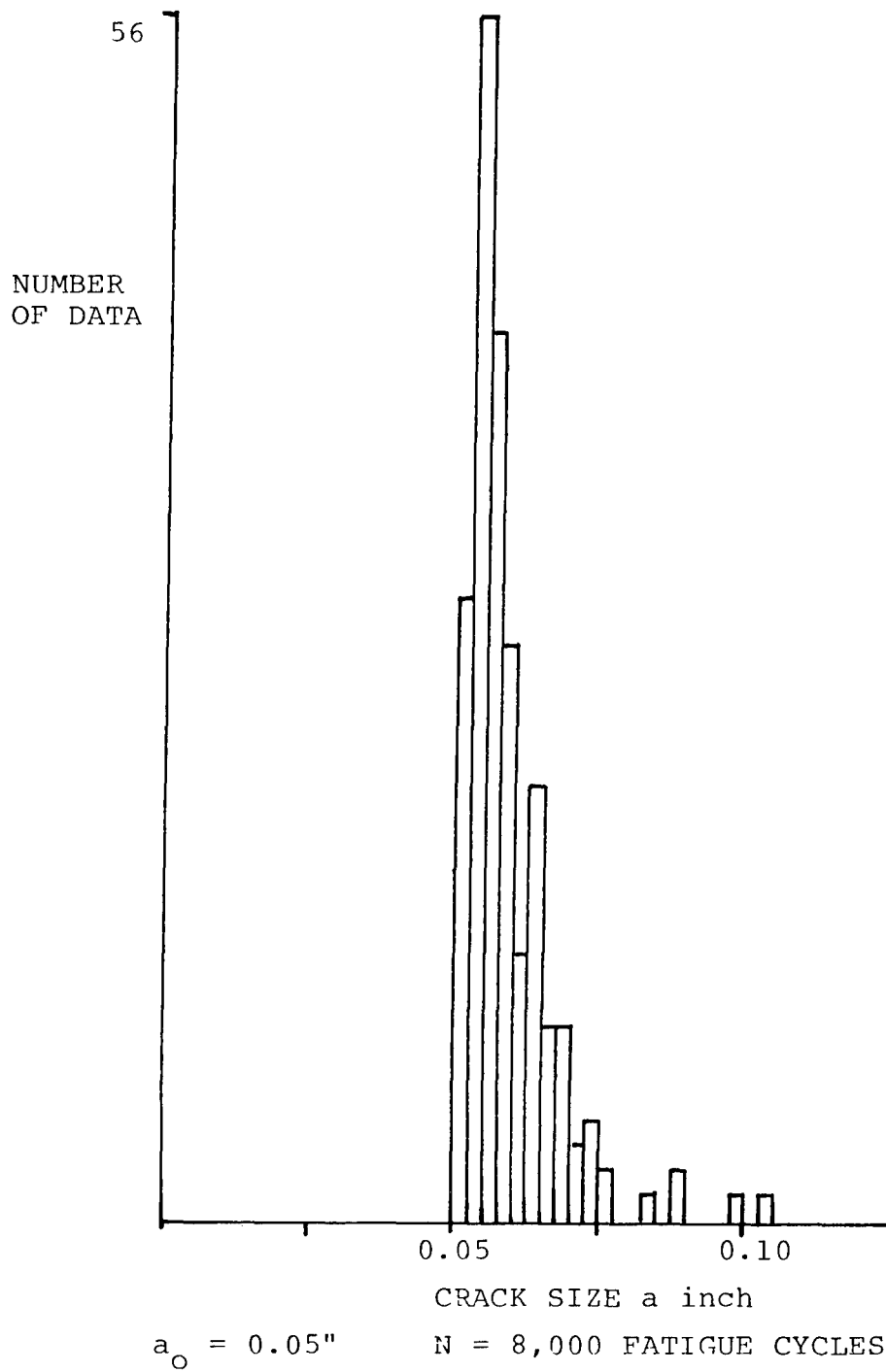


Figure 23: Crack Size Histogram ($a_i = .05$, $N = 8,000$)

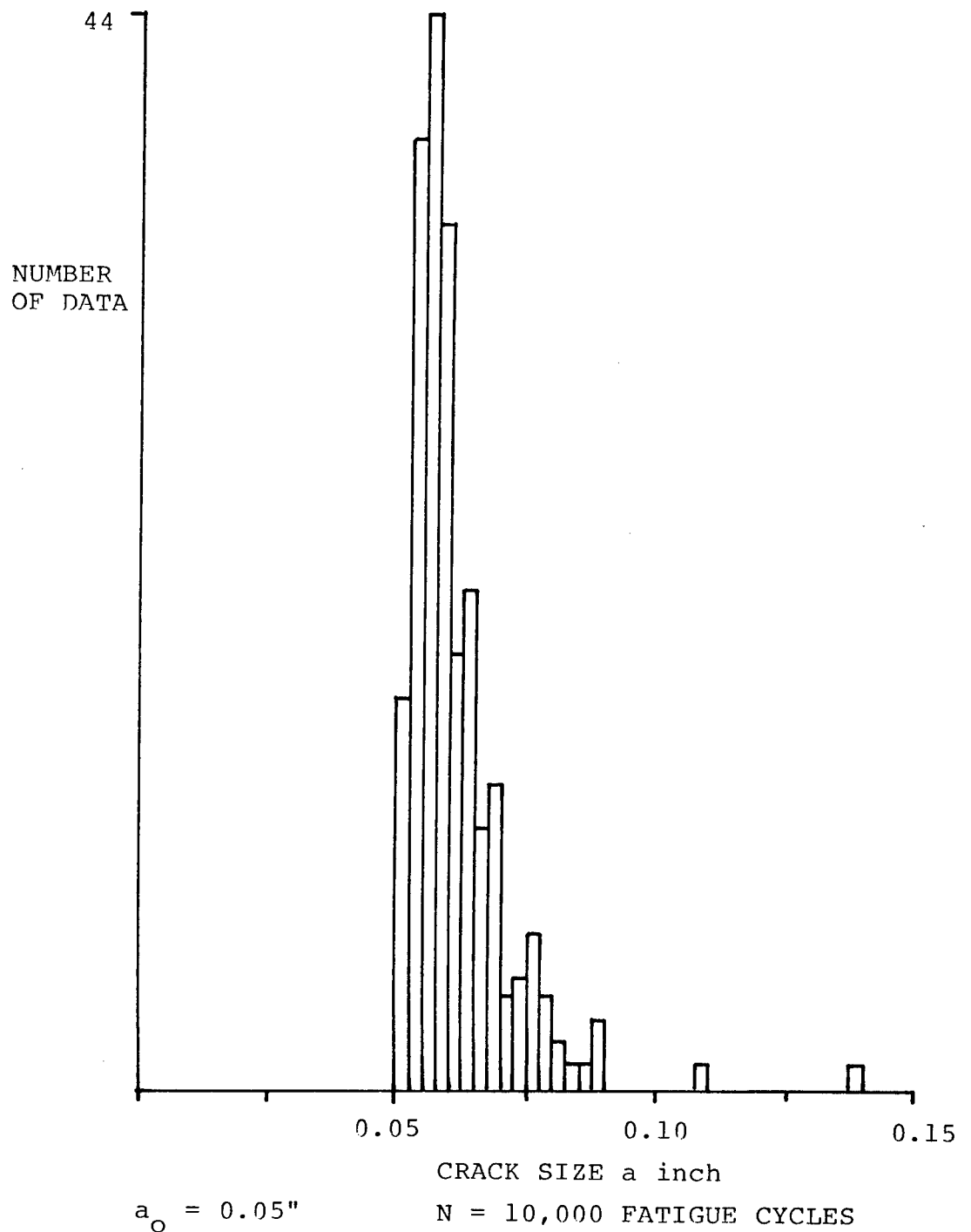


Figure 24: Crack Size Histogram ($a_i = .05$, $N = 10,000$)

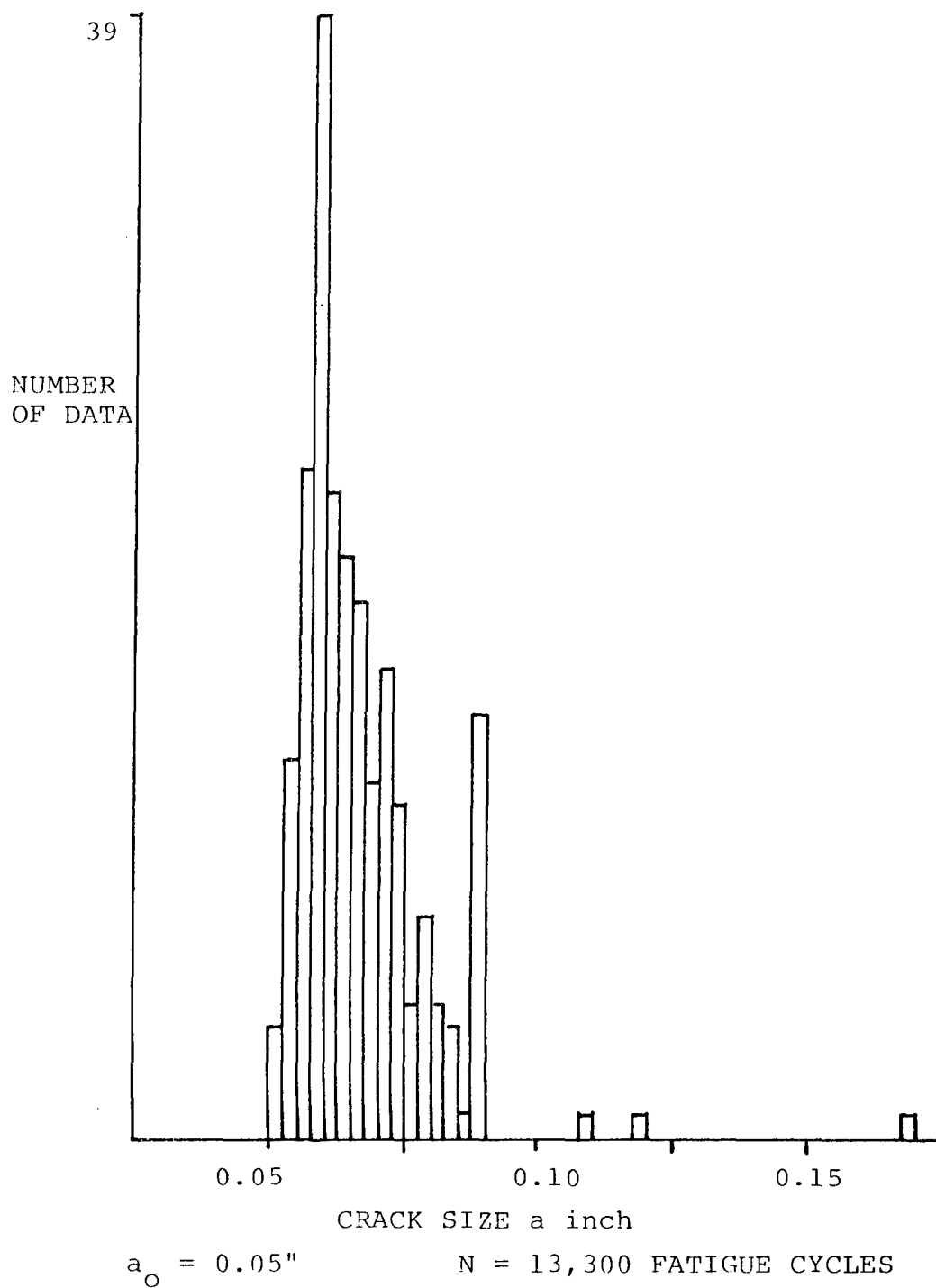


Figure 25: Crack Size Histogram ($a_i = .05$, $N = 13,300$)

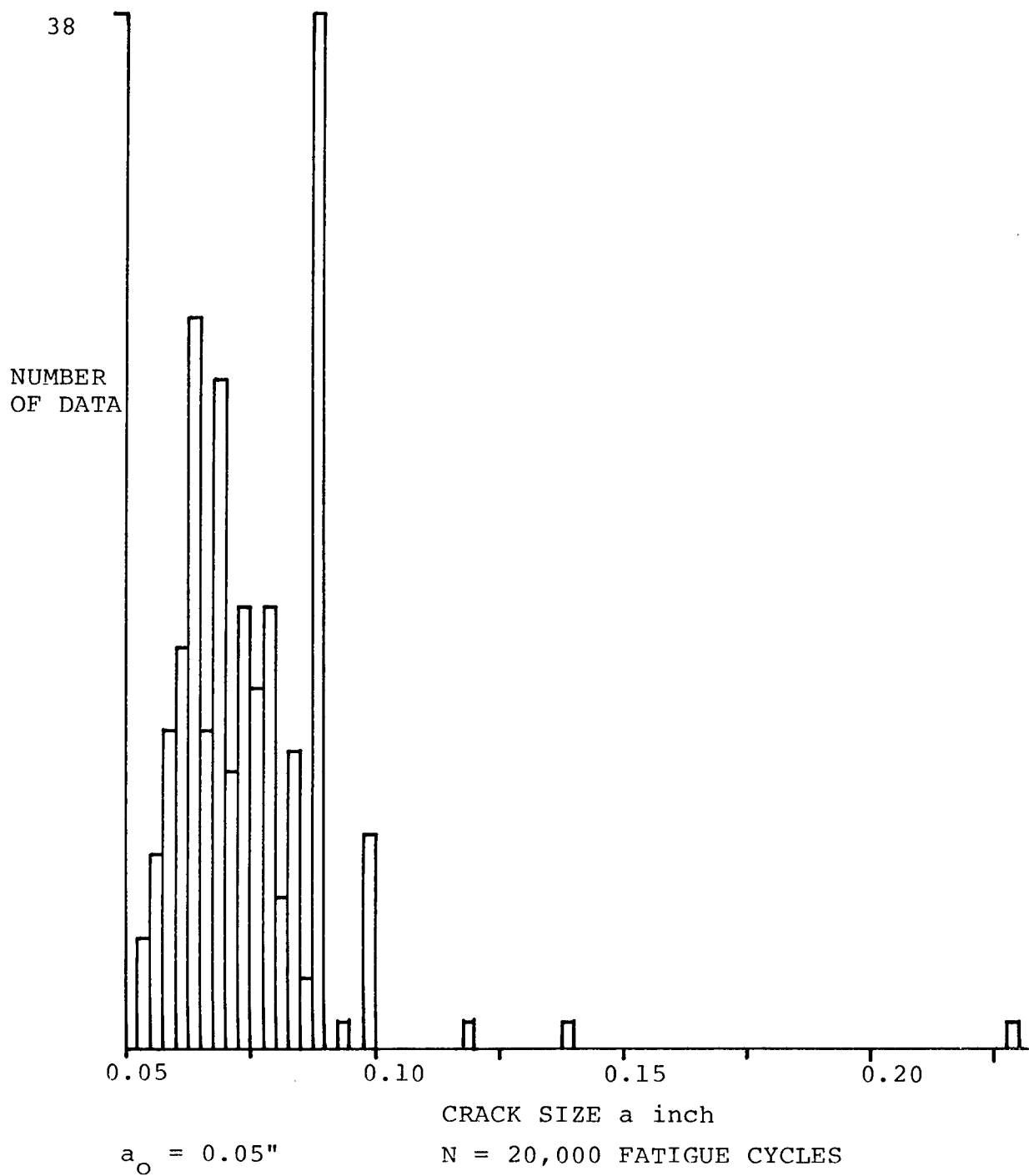


Figure 26: Crack Size Histogram ($a_i = .05$, $N = 20,000$)

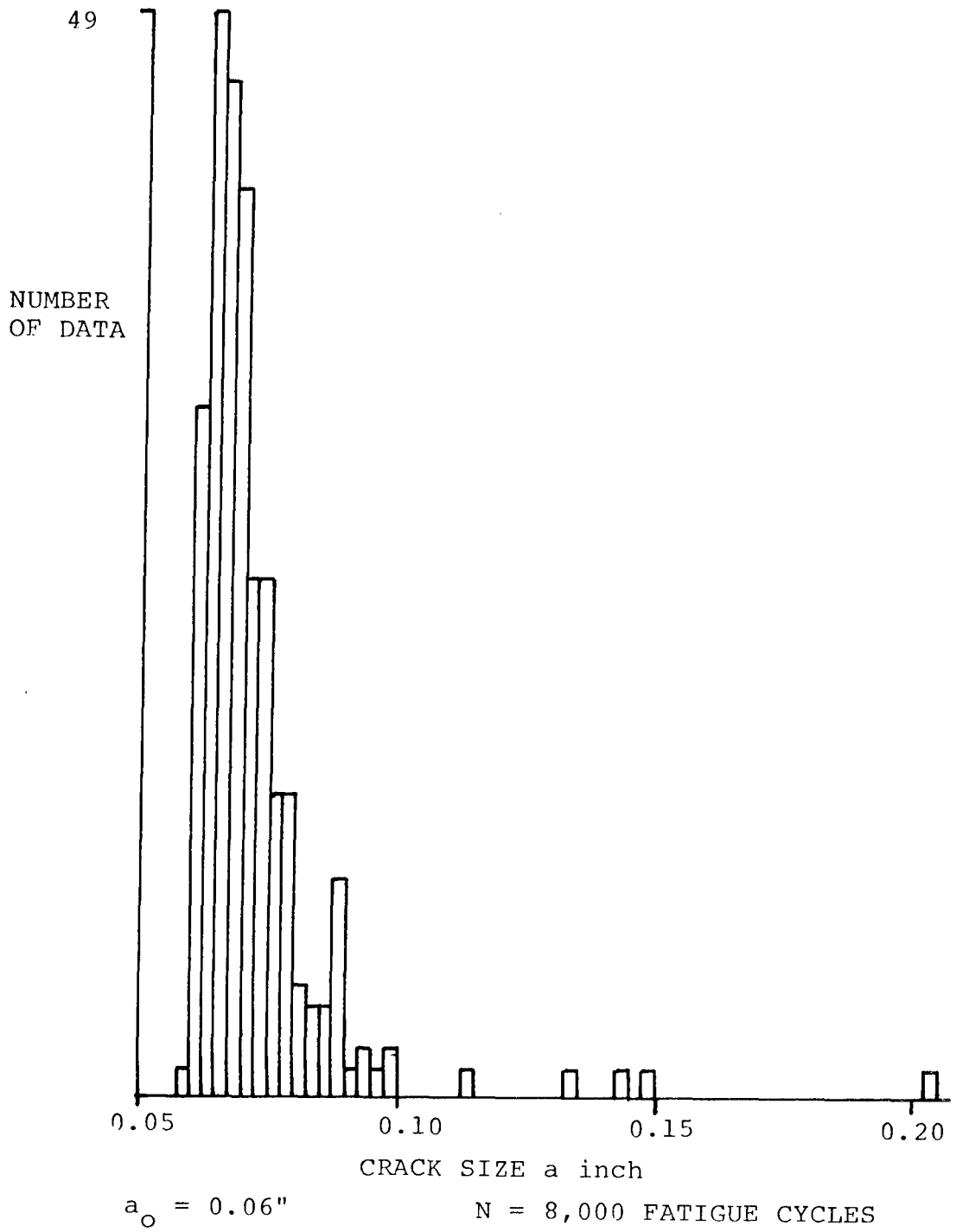


Figure 27: Crack Size Histogram ($a_i = .06$, $N = 8,000$)

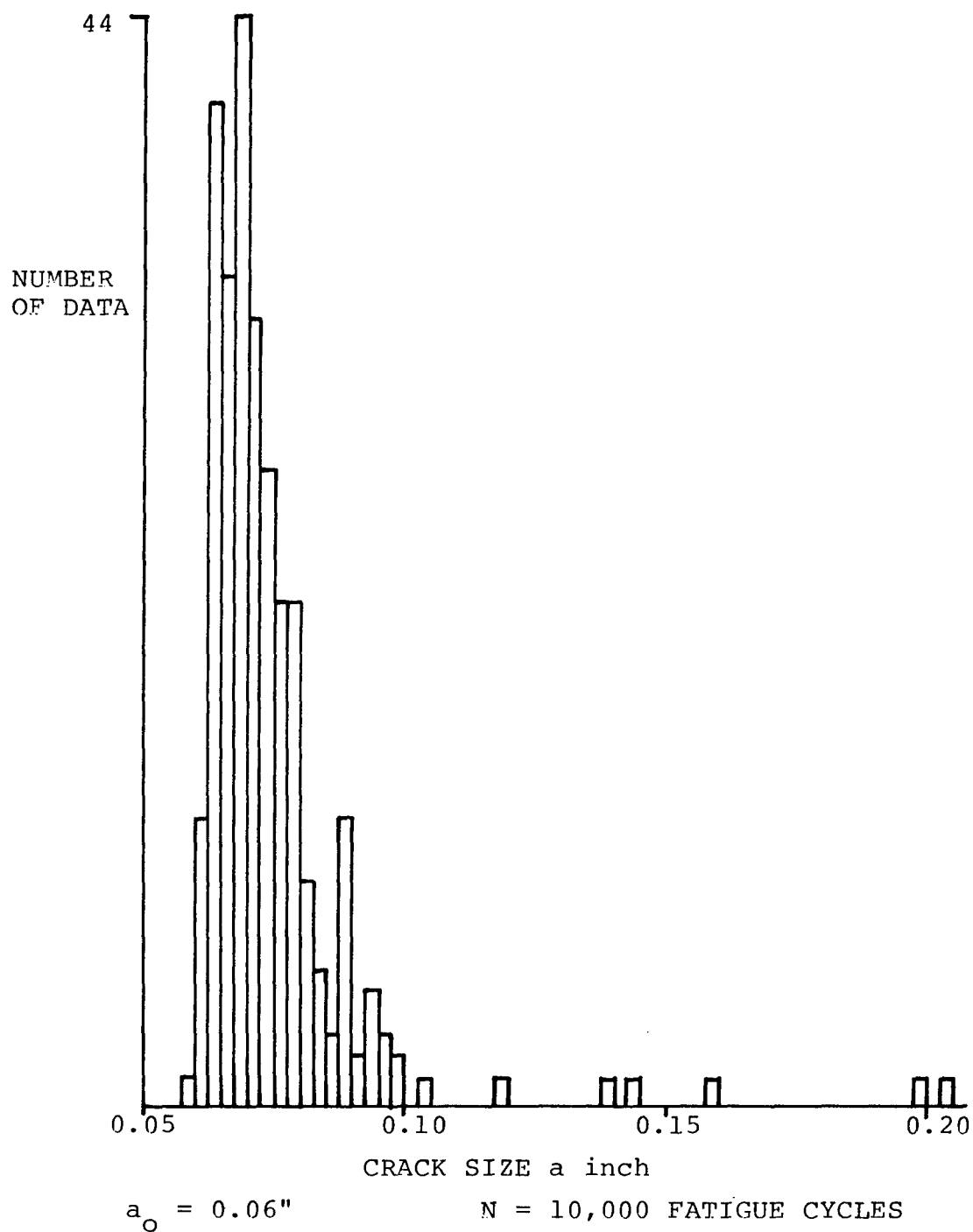
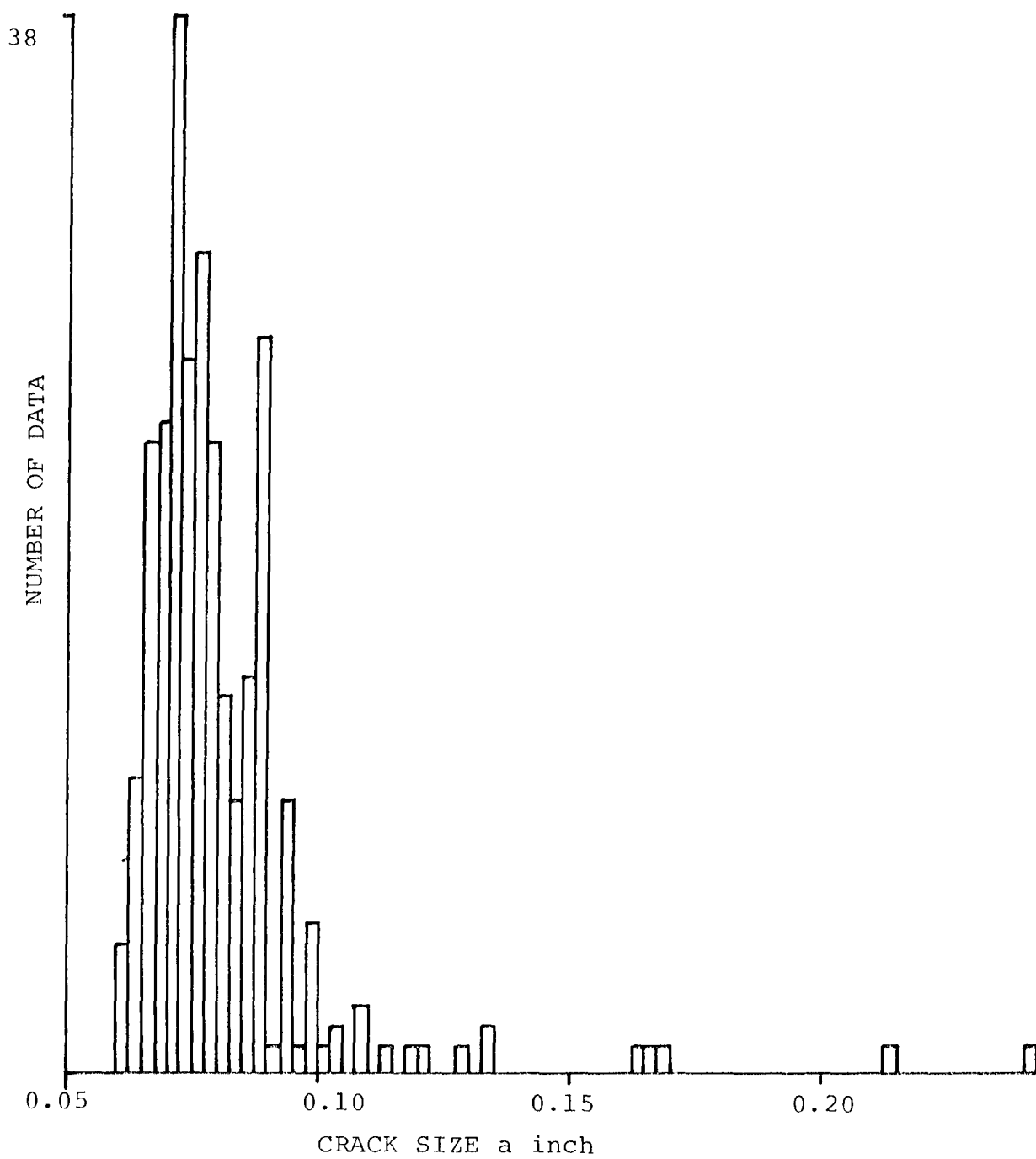


Figure 28: Crack Size Histogram ($a_i = .06$, $N = 10,000$)



$a_0 = 0.06"$

$N = 13,300$ FATIGUE CYCLES

Figure 29: Crack Size Histogram ($a_i = .06$, $N = 13,300$)

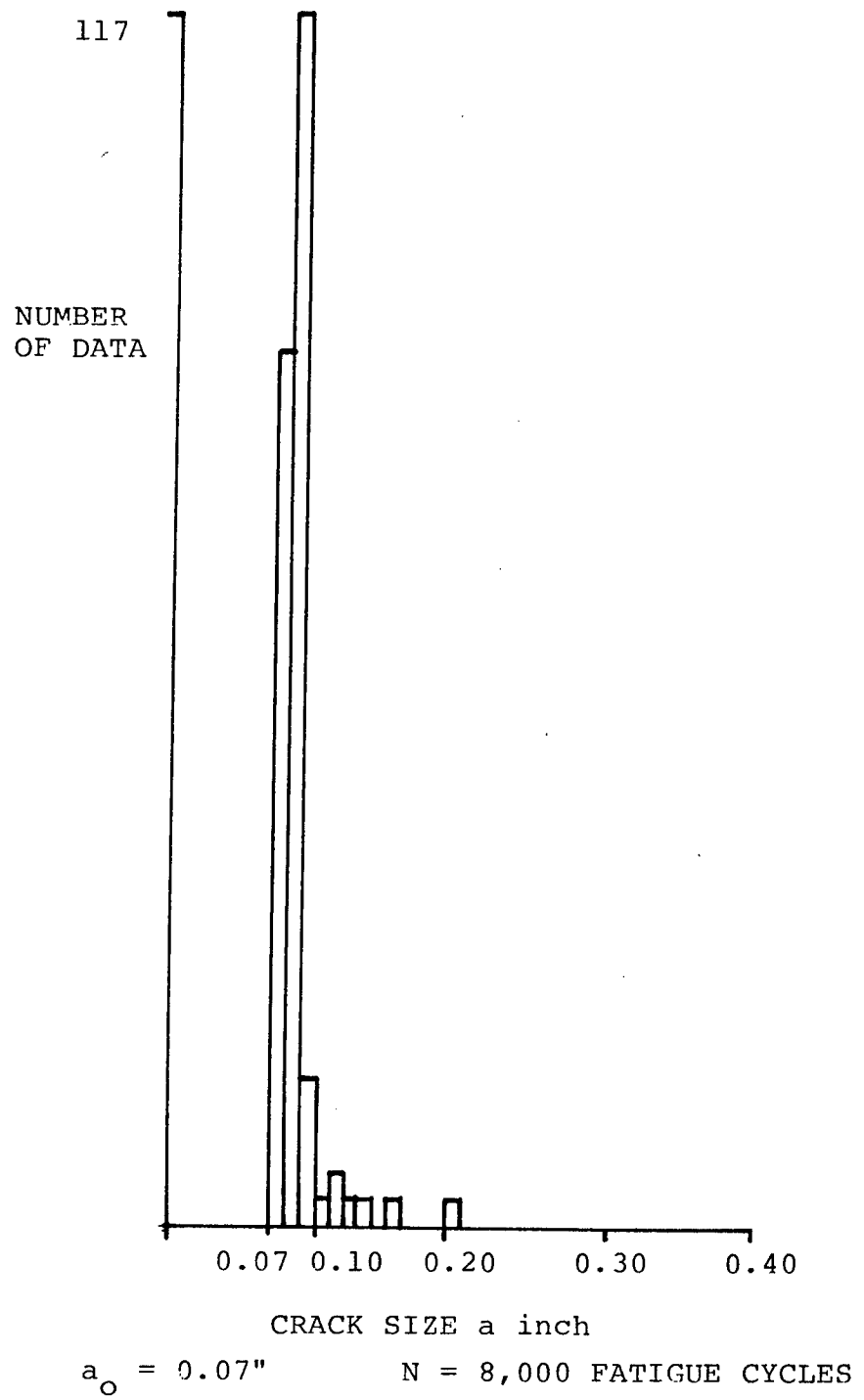


Figure 30: Crack Size Histogram ($a_i = .07$, $N = 8,000$)

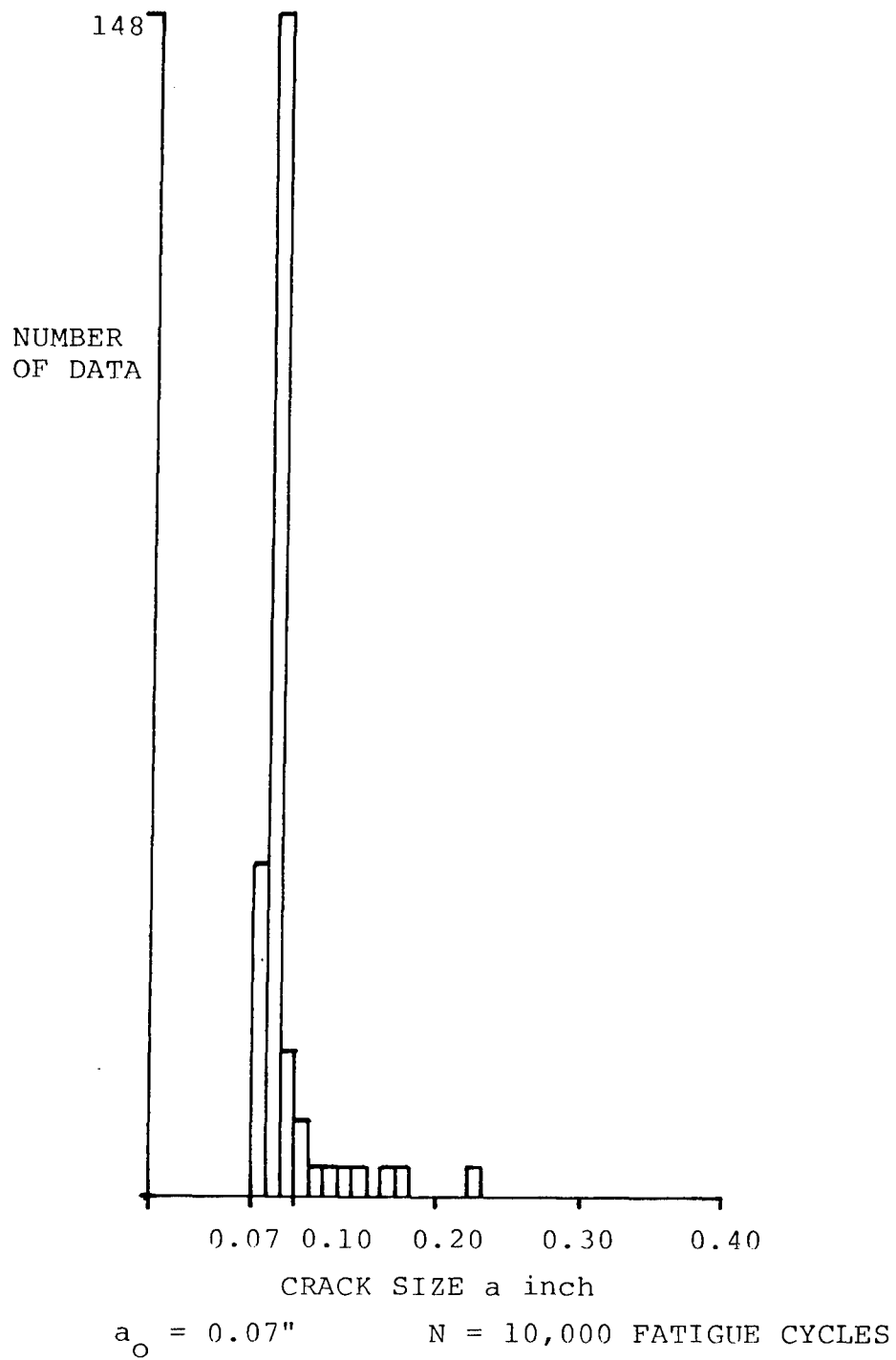


Figure 31: Crack Size Histogram ($a_i = .07$, $N = 10,000$)

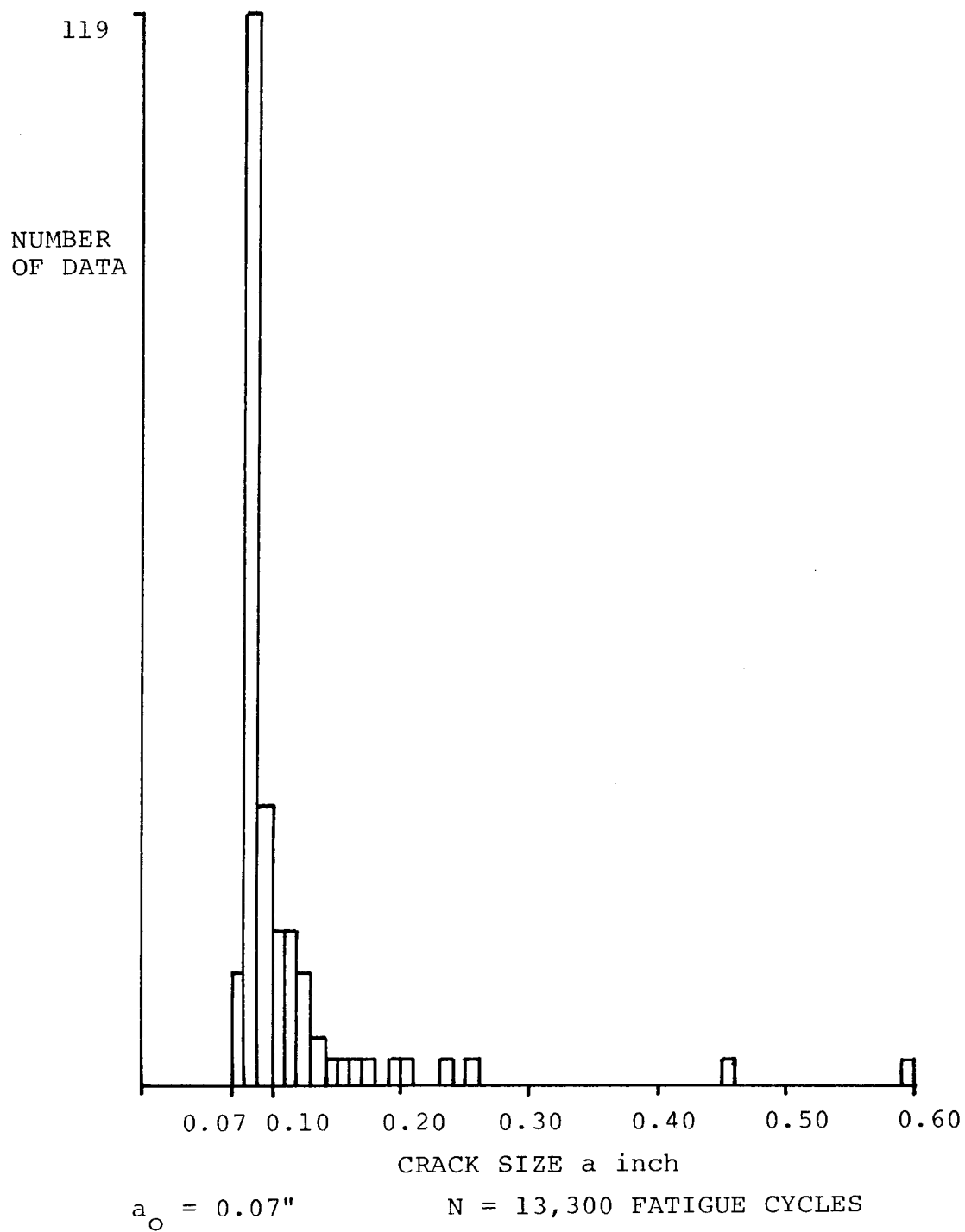


Figure 32: Crack Size Histogram ($a_i = .07$, $N = 13,300$)

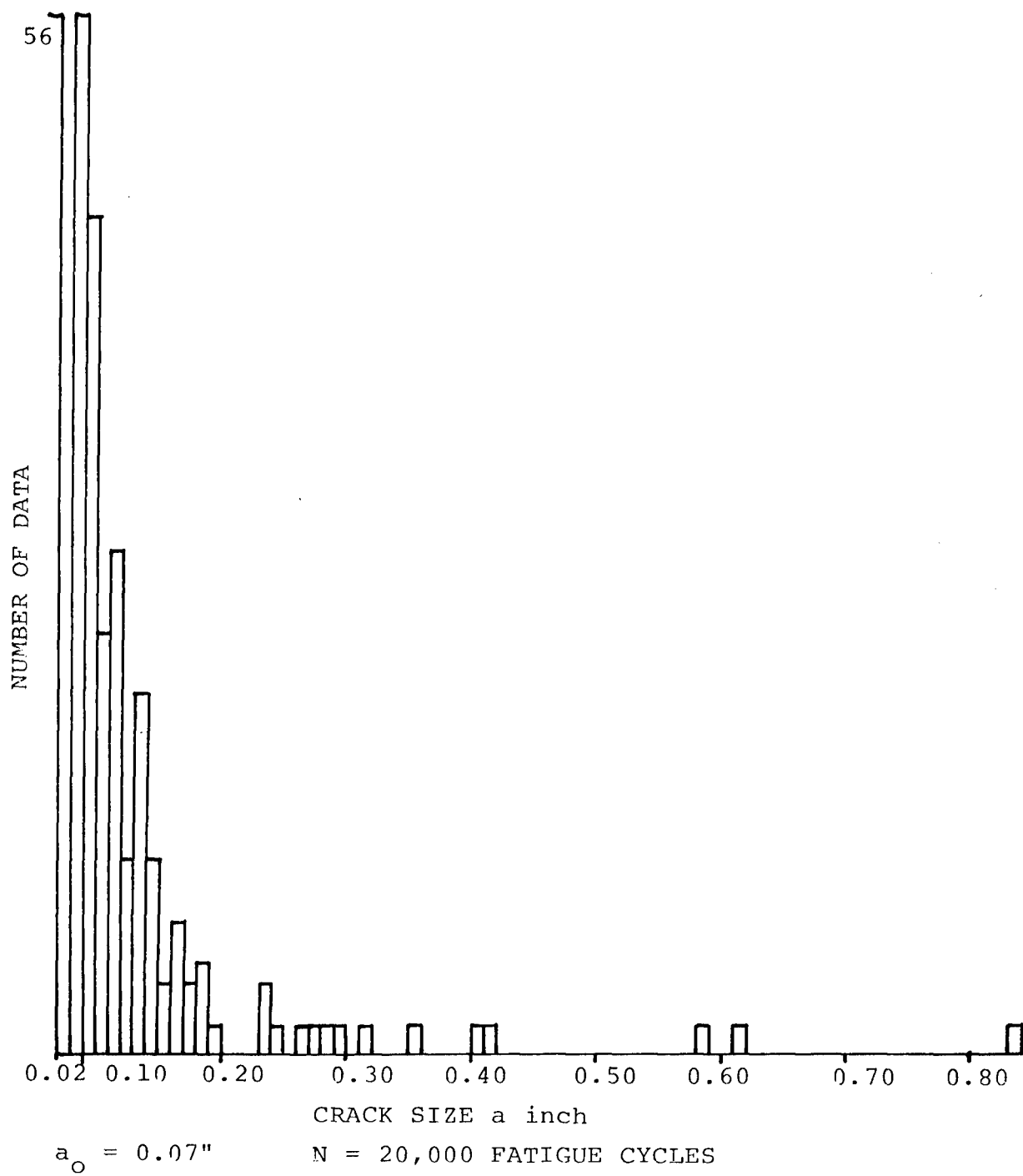


Figure 33: Crack Size Histogram ($a_i = .07$, $N = 20,000$)

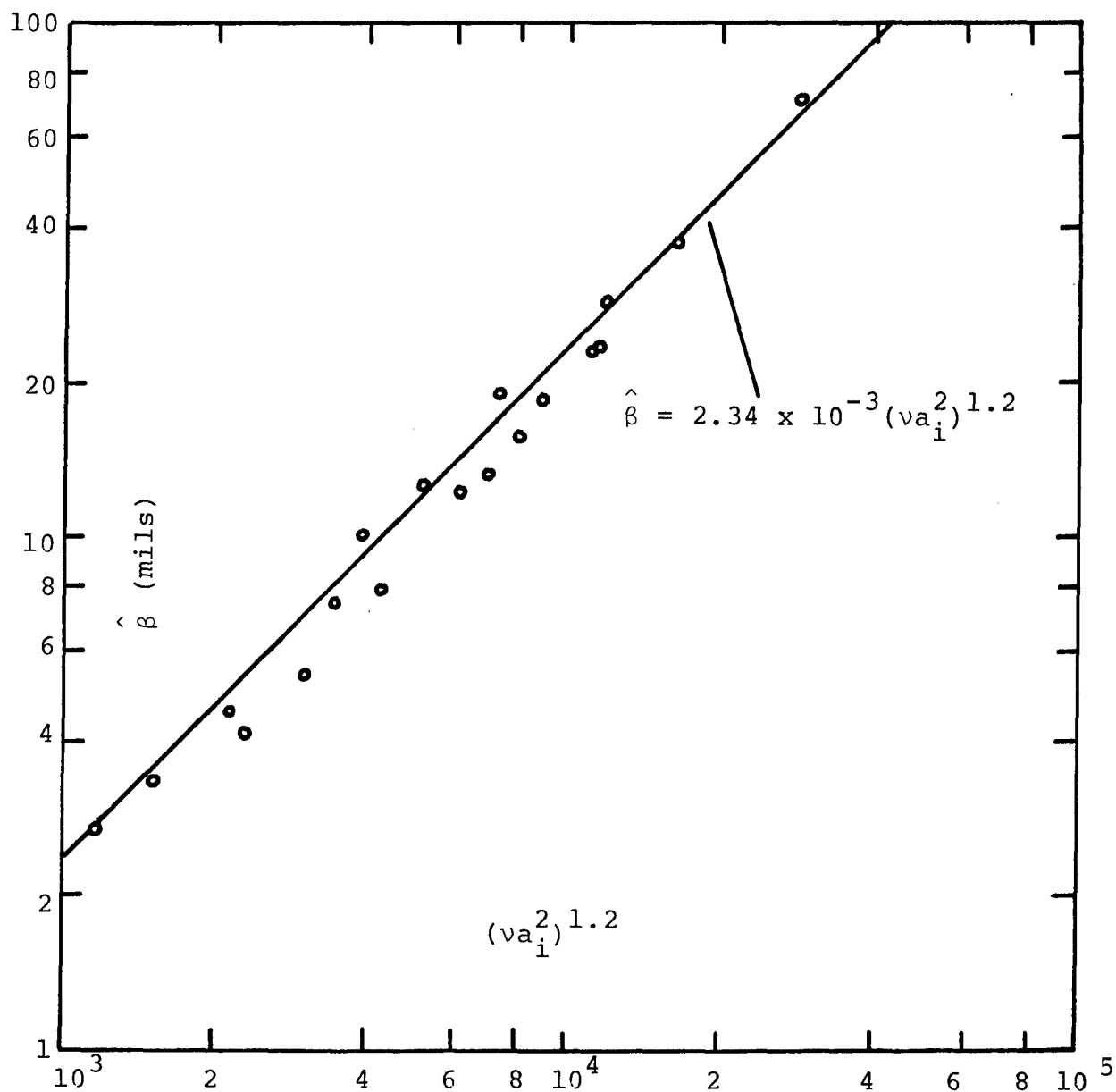


Figure 34: Correlation of Final Crack Size Distribution Parameters

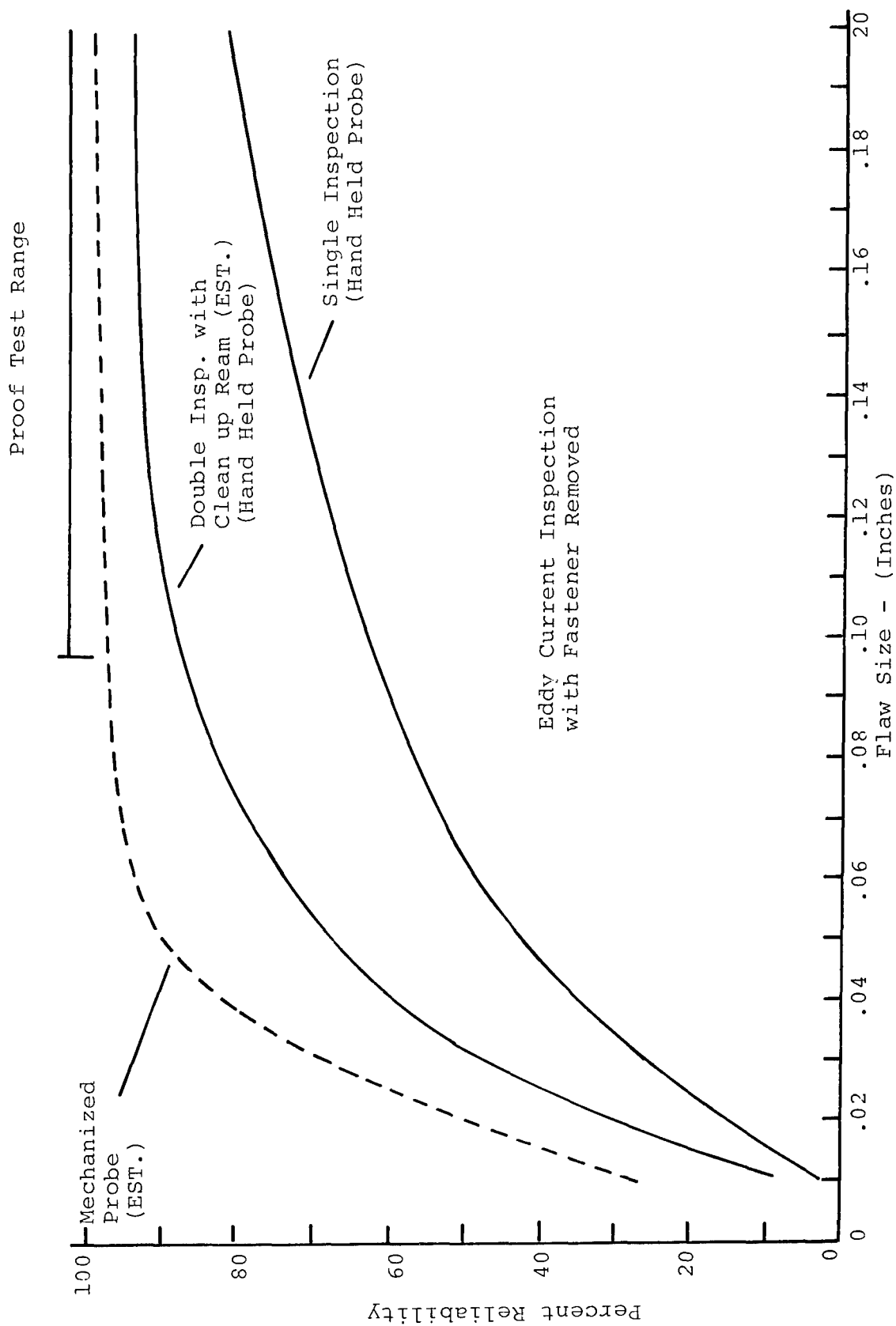


Figure 35: Typical Detection Probability Curves

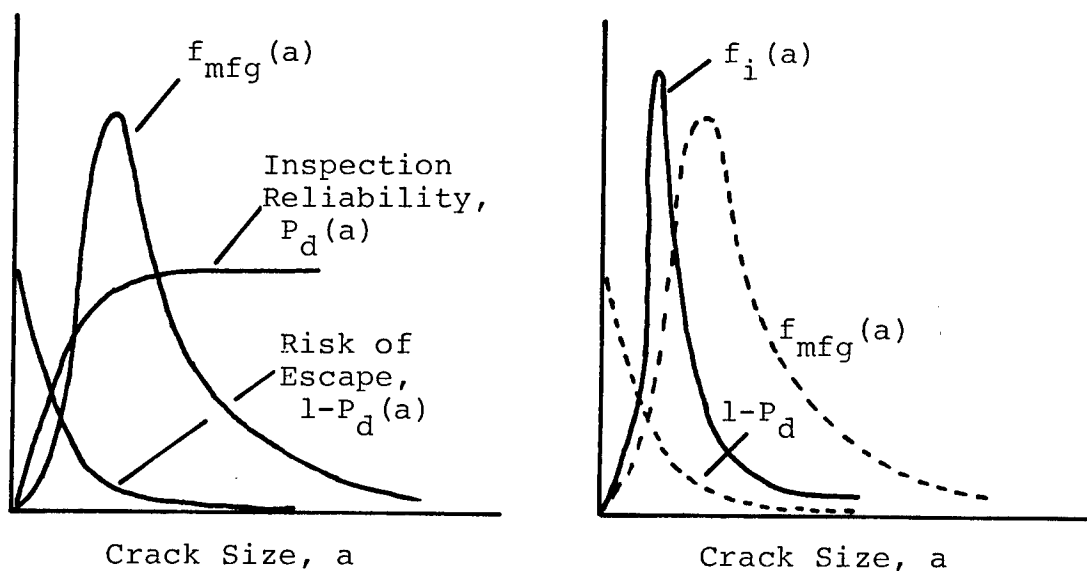


Figure 36: Reshaping of Flaw Creation Probability by Inspection Reliability

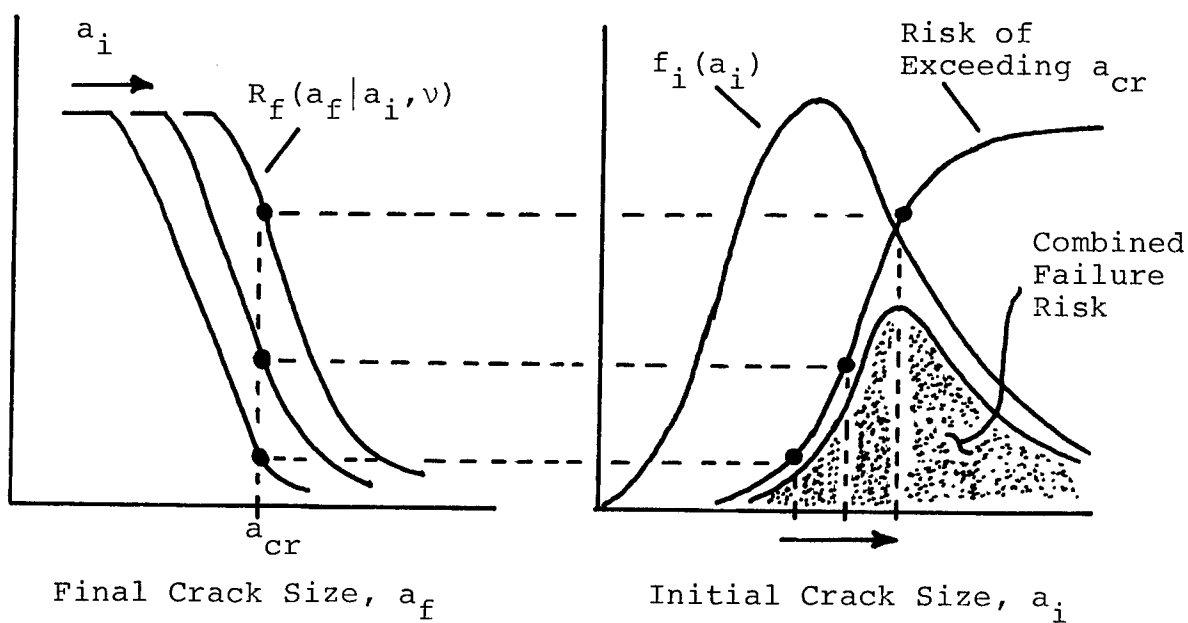


Figure 37: Schematic for Computation of Combined Failure Risk